AD_____

Award Number: DAMD17-01-1-0093

TITLE: Cell Motility in Tumor Invasion

PRINCIPAL INVESTIGATOR: Alan Wells, M.D.

CONTRACTING ORGANIZATION: University of Pittsburgh
Pittsburgh, Pennsylvania 15260

REPORT DATE: July 2003

TYPE OF REPORT: Annual

PREPARED FOR: U.S. Army Medical Research and Materiel Command
Fort Detrick, Maryland 21702-5012

DISTRIBUTION STATEMENT: Approved for Public Release;
Distribution Unlimited

REPORT DOCUMENTATION PAGE

Form Approved
OMB No. 074-0188

1. AGENCY USE ONLY (Leave blank)	2. REPORT DATE	3. REPORT TYPE AND DATES COVERED
	July 2003	Annual (1 Jul 02 - 30 Jun 03)

4. TITLE AND SUBTITLE
Cell Motility in Tumor Invasion

5. FUNDING NUMBERS
DAMD17-01-1-0093

6. AUTHOR(S)
Alan Wells, M.D.
Douglas A. Lauffenburger, Ph.D.
Timothy Turner, Ph.D.

7. PERFORMING ORGANIZATION NAME(S) AND ADDRESS(ES)
University of Pittsburgh
Pittsburgh, Pennsylvania 15260

E-Mail: wellsa@msx.upmc.edu

8. PERFORMING ORGANIZATION REPORT NUMBER

9. SPONSORING / MONITORING AGENCY NAME(S) AND ADDRESS(ES)
U.S. Army Medical Research and Materiel Command
Fort Detrick, Maryland 21702-5012

10. SPONSORING / MONITORING AGENCY REPORT NUMBER

11. SUPPLEMENTARY NOTES

12a. DISTRIBUTION / AVAILABILITY STATEMENT
Approved for Public Release; Distribution Unlimited

12b. DISTRIBUTION CODE

13. ABSTRACT (Maximum 200 Words)

Our overall objective is to understand how dysregulation of cell migration contributes to tumor cell invasiveness in prostate cancer. A combination of correlative epidemiological studies and basic experimental investigations demonstrate a role for upregulated EGF receptor (EGFR) signaling of motility in tumor progression. EGFR-mediated cell motility has been demonstrated to be critical for tumor invasion. *Our central premise is that prostate tumor cell invasiveness can be inhibited by interfering with the specific motility-associated calpain activation that governs the critical underlying biophysical process of de-adhesion.* Prior work has shown that integrin/matrix binding and growth factor stimulation jointly regulate cell locomotion. These studies have identified cell/substratum adhesiveness, especially the ability of a cell to detach at its trailing edge, as a primary governor of cell locomotion. We have recently found that this tail detachment is regulated by calpain activation. We are employing a set of model prostate tumor cell lines including a panel of syngeneic androgen-independent DU-145 cells that vary in invasiveness. Our findings in the first year showed that disruption of calpain activation and de-adhesion can block tumor invasiveness in vitro. This has been extended in the second year to demonstrate that this also applies in animal models of tumor invasiveness.

14. SUBJECT TERMS
Tumor progression, invasion, prostate cancer, EGF receptor, calpain, Cell motility, migration

15. NUMBER OF PAGES
55

16. PRICE CODE

17. SECURITY CLASSIFICATION OF REPORT	18. SECURITY CLASSIFICATION OF THIS PAGE	19. SECURITY CLASSIFICATION OF ABSTRACT	20. LIMITATION OF ABSTRACT
Unclassified	Unclassified	Unclassified	Unlimited

Table of Contents

CELL MOTILITY IN TUMOR INVASION

Alan Wells, Douglas Lauffenburger, Timothy Turner

INTRODUCTION

Our overall objective is to understand how dysregulation of cell migration contributes to tumor cell invasiveness in prostate cancer. A combination of correlative epidemiological studies and basic experimental investigations demonstrate a role for upregulated EGF receptor (EGFR) and other receptor signaling of motility in tumor progression. Especially in prostate tumor cells, EGFR-mediated cell motility has been demonstrated to be critical for tumor invasion. Since signals from extracellular matrix through integrins and from cell-cell contacts also strongly influence cell motility, the underlying common biophysical processes and biochemical controls of motility offer an attractive target for limiting tumor progression.

Our central premise is that prostate tumor cell invasiveness can be inhibited by interfering with the specific motility-associated calpain activation that governs the critical underlying biophysical process of de-adhesion. Prior work by ourselves and others has shown that integrin/matrix binding and growth factor stimulation jointly regulate cell locomotion. These studies have identified cell/substratum adhesiveness, especially the ability of a cell to detach at its trailing edge, as a primary governor of cell locomotion. We have recently found that this tail detachment is regulated by calpain activation. We will employ a set of model prostate tumor cell lines including the moderately invasive androgen-independent PC3 cell and its highly metastatic variant PC3M cell, along with a panel of syngeneic androgen-independent DU-145 cells that vary in invasiveness. We will determine whether targeted disruption of calpain activation and de-adhesion can block tumor invasiveness.

BODY

The original Statement of Work (Table 1) described a series of tasks to accomplish the two Objectives proposed and the additional training Objective. We have tackled these Tasks in the order of greatest yield so that work in areas can progress as systems are being optimized in others. The main efforts during the second year of this three-year project have been focused on the prostate tumor cell invasion in vivo and on adhesive surfaces and developing trainees. The progress during these first two years has put us in good position to accomplish the tasks within the time-frame provided.

Table 1. Original Statement of Work

Work to be performed at University of Pittsburgh (A. Wells Laboratory):

1. determine whether calpain is activated by growth factors and integrins in prostate cancer cells
2. determine whether calpain is limiting for prostate tumor cell motility on complex surfaces
3. determine whether prostate tumor cell transmigration of extracellular matrices is dependent on calpain activity
4. determine whether inhibition of calpain limits tumor invasiveness and metastasis in murine models of progressive prostate cancer

Work to be performed at MIT (D.A. Lauffenburger Laboratory):

1. determine optimal adhesiveness and high and low adhesiveness surfaces for fibroblast motility
2. test prostate tumor cell motility on defined adhesiveness surfaces

3. determine whether calpain activation is required for prostate cell motility

Work to be performed in partnership with Tuskegee (T. Turner Laboratory):
1. trainees will perform prostate cell growth and motility assays at Tuskegee and UPitt
2. trainees will perform in vivo mouse assays at UPitt

Work to be performed at University of Pittsburgh:

Task 1. determine whether calpain is activated by growth factors and integrins in prostate cancer cells. We found that EGF induces calpain activity in DU-145 prostate cancer cells (Fig 1; calpain activity in individual cells is shown by Boc fluorescence). Whether this activation is dependent on select substrata interaction withspecific integrins will be examined in year 3.

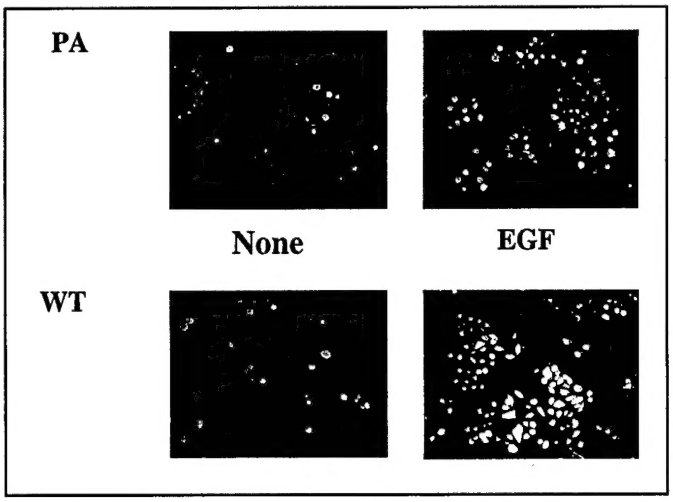

Task 2. determine whether calpain is limiting for prostate tumor cell motility on complex surfaces. Our data, generated during Year 1, demonstrated that calpain inhibitor I and leupeptin can limit DU-145 motility across self-generate matrix (Fig 2; bars showing migration in arbitrary units). This suggested that calpain could be targeted to limit tumor cell invasion by blocking migration. During year 3 we will determine whether integrin-mediated haptokinesis also depends upon calpain activation.

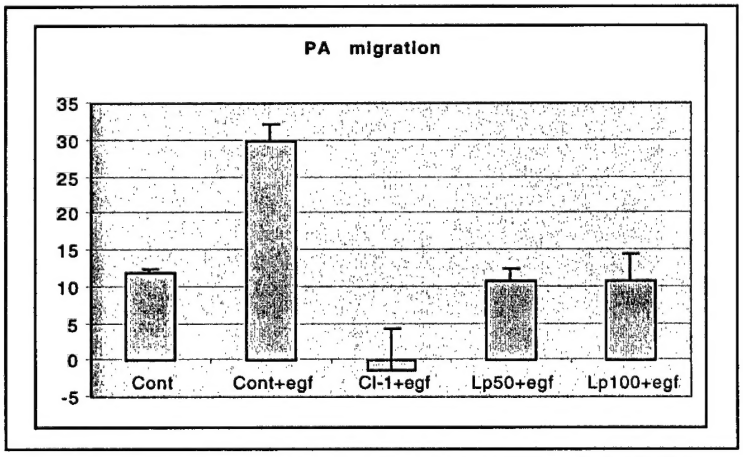

Task 3. determine whether prostate tumor cell transmigration of extracellular matrices is dependent on calpain activity. This task has been completed. In vitro transmigration of a Matrigel matrix by both Parental and WT EGFR-expressing DU-145 cells is blocked by inhibitors of calpain, CI-I and leupeptin (Fig 3). Furthermore, antisense downregulation of M-calpain limits this transmigration, providing specificity (Fig 4, below).

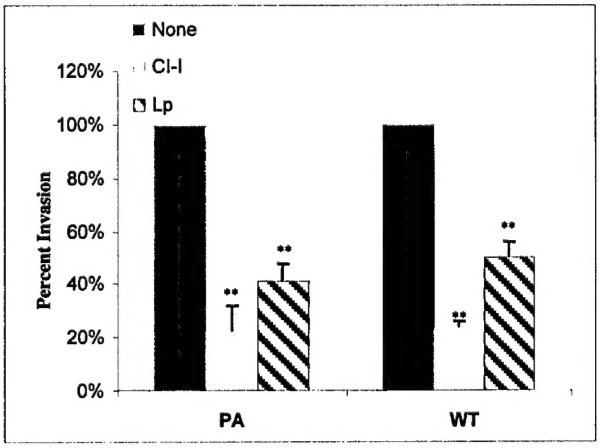

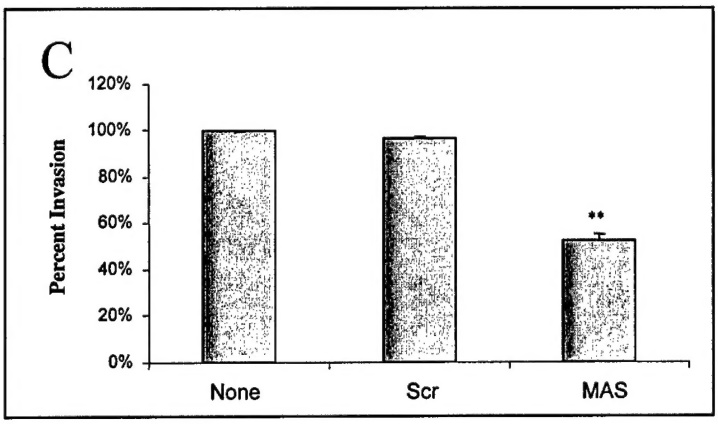

Task 4. determine whether inhibition of calpain limits tumor invasiveness and metastasis in murine models of progressive prostate cancer. We challenged mice with DU-145 prostate carcinoma tumor xenografts with inhibitors of calpain. Tumor invasiveness was reduced in the presence of daily injections of the inhibitor leupeptin (Table 1). The differences invasiveness between treated and mock treated were significant ($P < 0.05$) by T-test and ANOVA analyses.

	PA+HBSS	PA+Leupeptin	WT+HBSS	WT+leupeptin
Diaphragm tumors	14/14	13/14	14/14	13/14
Diaphragm invasiver	1.71	0.7**	2.35	1.25*

Antisense constructs to m-calpain were expressed stably in DU-145 cells. These also limited tumor invasion into the diaphragm of mice (Table 2). This task is completed.

	V PA DU145	C2AS PA DU145	V WT DU145	C2AS WT DU145
Diaphragm tumors	9/10	8/10	4/5	3/5
Diaphragm invasiver	2.33	1.13*	3.50	1.67^

<u>*Work to be performed at MIT:*</u>
Task 5. determine optimal adhesiveness and high and low adhesiveness surfaces for fibroblast motility. This task was completed in year 1, and is covered in the previous yearly update.

Task 6. test prostate tumor cell motility on defined adhesiveness surfaces. In order to generate most cost-effectively, rapidly, and reproducibly quantitative measurements of cell/substratum adhesion across multiple conditions of cell types, substratum coating compositions and levels, and medium compositions and concentrations, we have developed a new microfluidic assay for cell adhesion. This involves constructing a device with multiple parallel channels possessing different widths and lengths, which then offers a spectrum of fluid shear stresses simultaneously for each of a set of experimental conditions and requiring minimal volumes of media and substratum surface areas. We have recently validated it for EGFR signaling-dependent de-adhesion in our NR6 fibroblast model across a range of fibronectin concentrations [H. Lu, L. Koo, D. Lauffenburger, L. Griffith, K. Jensen (manuscript in preparation)]. In year 3, we will

apply this novel device to the DU-145 and PC3 cells under the set of conditions relevant for this grant: fibronectin-coated surfaces (at 0.1, 0.3, 1, and 3 ug/ml coating).

We need to test this in the presence and absence of EGF and EGFR inhibitors to examine effects of both paracrine and autocrine EGFR signaling. Because autocrine EGFR signaling is operative in prostate cancers, we are quantifying the autocrine ligand release and capture characteristics of the DU-145 and PC3 cells using a method developed previously in the Lauffenburger laboratory [Dewitt, A., J.Y. Dong, H.S. Wiley, and D.A. Lauffenburger, "Quantitative Analysis of the EGF Receptor Autocrine System Reveals Cryptic Regulation of Cell Response by Ligand Capture", J. Cell Sci. 114: 2301-2313 (2001)]. Figure 5 (below) shows production of TGFα in DU-145 parental cells. The slope of the upper curve characterizes the rate of autocrine TGFα released into the media when EGFR are blocked by a monoclonal antibody while the slope of the lower curve characterizes the rate of autocrine TGFα released when EGFR are not blocked. These two slopes enable determination of the rate of autocrine ligand production, in this case ~1 molecule/cell-min, along with the percentage of ligand captured by the cell receptors, in this case ~99%. Thus, an autocrine circuit stimulating EGFR signaling operates in these cells but would be very difficult to "see" without experimental intervention since very little ligand escapes into the medium under normal conditions. We have performed similar experiments for the DU-145 WT cells and the PC3 cells; the latter produce autocrine TGFα at roughly 10x the rate of the DU-145 cells (A. Kitay, A. Wells, and D.A. Lauffenburger, in preparation).

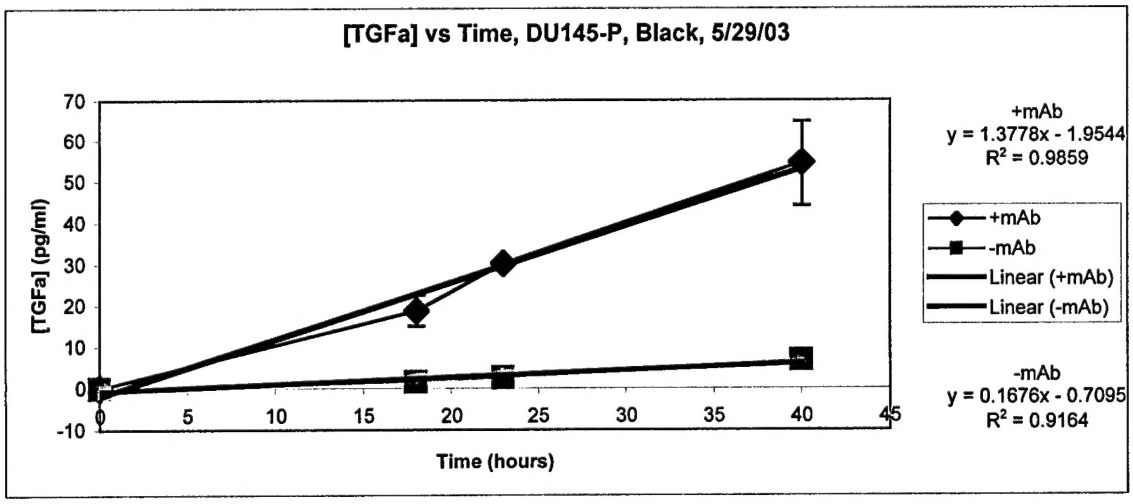

Task 7. determine whether calpain activation is required for prostate cell motility. This was completed during year 2 in conjunction with work at UPitt (Fig 2, above).

Work to be performed in partnership with Tuskegee:
Task 8. trainees will perform prostate cell growth and motility assays at Tuskegee and UPitt. Masters students Clayton Yates and Karlyn Bailey have been trained at Tuskegee to perform these assays with the DU-145 human prostate tumor lines. Clayton Yates has transitioned to University of Pittsburgh as a PhD degree student in the Cellular and Molecular Pathology graduate program. Clayton Yates is now a thesis candidate, and has focused on prostate cancer

cell-cell cohesion as a key determinant for metastatic growth. Ms. Bailey has been performing cell growth assays in the presence of EGFR and LHRH inhibitors at Tuskegee.

Task 9. trainees will perform in vivo mouse assays at UPitt. Mr. Yates learned the in vivo mouse tumor growth and invasion assays. More importantly, he has developed an ex vivo metastasis model of tumor cell growth in a liver bioreactor. Mr. Yates has learned to generate the liver bioreactor and seed it with prostate tumor cells.

KEY RESEARCH ACCOMPLISHMENTS

- EGFR signaling enhances prostate tumor motility
- EGFR signaling increases calpain activity in prostate cancer cells
- Calpain inhibitors block prostate tumor invasiveness in vitro
- Calpain inhibitors block prostate tumor invasiveness in vivo
- Downregulation of m-calpain limits prostate tumor invasiveness in vitro
- Downregulation of m-calpain limits prostate tumor invasiveness in vivo
- EGFR signaling enhances fibroblast motility over a narrow range of fibronectin adhesiveness
- One trainnee successfully transitioned from Tuskegee Masters program to be a doctoral thesis candidate at University of Pittsburgh
- The trainee developed a novel prostate tumor metastasis model in an ex vivo liver bioreactor

REPORTABLE OUTCOMES

Articles:

A Glading, DA Lauffenburger, A Wells (2002). Cutting to the chase: calpain proteases in cell motility. Trends in Cell Biology 12, 46-54. (Year 1)

A Wells, J Kassis, J Solava, T Turner, DA Lauffenburger (2002). Growth factor-induced cell motility in tumor invasion. Acta Oncologica 41, 124-130. (Year 1)

A Mamoune, JH Luo, DA Lauffenburger, A Wells. m-Calpain as a target for limiting prostate cancer invasion. Cancer Research, in press. (appended)

Abstracts:

A Mamoune, J Kassis, D Lauffenburger, A Wells (2002) Calpain inhibition reduces prostate tumor invasion. American Association for Cancer Research (AACR) Annual Meeting, San Francisco, CA (Year 1)

Clayton C. Yates, Karlyn J. Bailey, Alan Wells and Timothy Turner (2001). The Effects of the Luteinizing Hormone Releasing Hormone Antagonist, Cetrorelix on the Cell Adhesion Profile of an Invasive DU-145 Human Prostate Cell Line. Selected Abstract-5th Joint Conference of the American Association for Cancer Research and the Japanese Cancer Association, Maui, HI (Year 1)

Clayton C. Yates, Karlyn J. Bailey, Alan Wells and Timothy Turner (2001). Cetrorelix, a Luteinizing Hormone Releasing Hormone Antagonist, Influences the Cell Adhesion Profile of an Invasive DU-145 Human Prostate Cell Line. Selected Abstract-Keystone Symposium, Tahoe City, CA (Year 1)

H Lu, L Koo, D Lauffenburger, L Griffith, K Jensen (2002) Novel microfluidic device for high-throughput quantitative measurement of cell/substratum adhesion. DARPA Bio-Info-Micro Program annual meeting, San Francisco CA. (appended)

C Yates, D B Stolz, L Griffith, A Wells (2003) An organotypic model for prostate tumor metastasis. 94th Annual Meeting of the American Association for Cancer Research, Washington, DC (appended)

K J Bailey, A Hassan, A Wells, T Turner (2002) Protein kinase C signaling in the human prostate cancer cell line DU-145 after exposure to an LHRH analog. Research Centers in Minority Institutions (RCMI) 2002 Spring Symposium, Jackson, MS (appended)

Submitted Paper:
C Yates, A Wells, T Turner (2003) Luteinizing hormone releasing hormone (LHRH) antagonist reverses the cell adhesion profile of DU-145 human prostate carcinoma.

Training:
C Yates has been accepted as from Tuskegee University with a MA in Biology to a PhD candidate in the program in Cellular and Molecular Pathology at University of Pittsburgh.

CONCLUSIONS

The second year of this multiyear award has reached major defined milestones and established the base for increasing productivity over the final year of the award. It is has also highlighted new directions for further research.

Importance/Implications: The Key Accomplishments above firmly demonstrate the validity of the model of the tumor biology that calpain-mediated deadhesion is a rate-limiting step in tumor cell motility and invasion. This provide the 'proof a concept' that targeting calpain is a rationale therapeutic option. The implications are clear that calpain inhibitors, currently being developed for muscle-wasting conditions, may have a role as adjuvant cancer therapy to limit the spread of prostate carcinoma.

Furthermore, initial data suggest that cell-cell cohesion may be a rate-limiting process in prostate tumor metastasis. Work from others suggest that calpain may cleave cadherins in prostate cancer cells. Thus, we postulate that cell-cell cohesion is controlled by calpain cleavage of cadherins.

Recommended changes: The results to-date have nearly completed the key tasks. The findings on cell-cell cohesion have major implications for the regulation of tumor invasion and thus lead us to introduce this project along side the unfinished tasks in year 3.

REFERENCES

none

High-Throughput Microfluidic Shear Devices for Quantitative Analysis of Cell Adhesion

Hang Lu[1], Lily Y. Koo[1*], Wechung M. Wang[1],*
Douglas A. Lauffenburger[1,2], Linda G. Griffith[1,2], and Klavs F. Jensen[1,‡]

[1]Department of Chemical Engineering, [2]Division of Biological Engineering and Biotechnology Process Engineering Center,
Massachusetts Institute of Technology, Cambridge, MA 02139
[‡]Corresponding author: kfjensen@mit.edu

To be submitted to PNAS

*** These authors contributed equally.**

Abstract

We describe the design, construction, and characterization of new microfluidic systems for the study of cell adhesion and cell mechanics. The method, an adaptation of the laminar flow shear-induced detachment assay, offers multiple advantages over previous approaches, including a wide dynamic range of distractive forces, high-throughput performance, simplicity in experimental setup and experimental control, and the potential for integration with other micro-analytic modules. By manipulating the shape and surface chemistry of the flow channel network within devices, we are able to control both the hydrodynamic shear force and the biochemical activities for each of several channels independently. Employing these microfluidic cell-detachment devices, the dynamics of cell detachment under different conditions can be captured simultaneously using time-lapse videomicroscopy. We demonstrate quantitative assessment of cell adhesion to fibronectin-coated substrates in micro-channels, and show that the fraction of adherent cells is dependent on both the shear stress and fibronectin concentration. Furthermore, a combined perfusion-fluid shear device is designed to incorporate a medium replenishment system that maintains cell viability for long-term culture as well as to introduces exogenous reagents for cell adhesion studies. Results obtained using this device demonstrate that fibroblasts respond normally to epidermal growth factor (EGF) stimulation by reducing their adhesion strength to the substrate. These microfluidic devices can potentially be integrated with other microfluidic systems for cell lysis and analysis to provide insight into cellular and molecular mechanisms of cell adhesion.

Introduction

Adhesive interactions between cells and their physical environments are central in developmental biology, tissue maintenance, tissue engineering, cancer progression, and biotechnological processes. Several methods have been developed to measure cell-substrate adhesion strength by application of distractive forces to adherent cells. These adhesion assays can be classified according to the nature of the distractive force applied: hydrodynamic shear force (1-7), centrifugal (normal) force (8-10), and micromanipulation (11-14). However, the limitations of these currently available assays include low-throughput performance, cumbersome apparatus assembly, apparatus failure, and inadequate range of detachment forces. For example, the centrifugation assay can measure multiple cellular or biochemical events (10, 15, 16), but only one constant normal force can be applied in one experiment, and the magnitude of the force is severely constrained by equipment safety requirements. In contrast, in many shear force-based assays that utilize the tapered parallel plate flow chamber, rotating disks, or radial flow between parallel discs, generation of variable shear force within the same flow field in a single experiment is possible, but variation in biochemical and cellular parameters within a single experiment is limited. An alternative approach employs micromanipulation of single cells by using micropipettes or force-responsive microprobes to assess cell adhesion strength or bond strength. These micromanipulation experiments, while revealing features of individual cell behavior, are usually technique-intensive, low-throughput, and laborious if statistical results for a cell population as a whole are needed. To address some of the limitations faced by the conventional methods, we have designed a series of simple microfluidic devices fabricated using rapid prototyping techniques (17). Fig. 1A shows the general concept of such devices.

Micro systems have emerged as a means to improve throughput, resolution, and fidelity of measurements in many biological applications (18-24). We show that microfluidic systems also offer unique advantages in quantitative cell adhesion studies. The small dimensions associated with micron-sized channels ensure laminar flow even at very high fluid linear velocities (25), thereby allowing generation of relatively large shear stresses. This is an important feature because many existing adhesion assays are limited by the practical range of applied forces achievable. For example, the centrifugation assay failed to provide sufficient force to dislodge cells as soon as 15-minute post-seeding at 37 °C (26). Conventional shear force-based assays are

often limited to hundreds of dynes/cm^2 (1, 5, 7, 27). Therefore, it remains a challenge to detach and analyze strongly and fully adherent cells such as fibroblasts or hepatocytes, which may require detachment forces that are greater than 10^3 dynes/cm^2 (28, 29). In addition, the microfluidic devices only require small amount of reagents (e.g. active biomaterials and soluble factors) and shearing fluids. These devices are readily operated in parallel for high-throughput experimentation compared to conventional methods.

By adopting rapid prototyping with poly(dimethylsiloxane) (PDMS), the turn-around time for designing, fabricating, and testing devices can be as fast as a day or two. Although PDMS surface properties are not studied as extensively as glass surfaces, many groups are working towards methods that can improve the surface properties (30-34). PDMS, being optically transparent, enables the use of different real-time microscopy techniques to explore cell behaviors under diverse experimental conditions. In this work, we use time-lapse videomicroscopy to capture the dynamics of cell detachment under multiple conditions simultaneously.

Using the microfluidic devices, we assess short-term cell adhesion as a function of the molecular density of fibronectin on the substrate, shear stress, and cell type. We also introduce microfluidic devices designed to allow long-term culture of mammalian cells and to accommodate introduction of exogenous reagents through continuous perfusion. As an example of the utility of these devices in addressing biologically relevant phenomena, we probe the effect of epidermal growth factor (EGF) on long-term cell adhesion, and demonstrate that the results obtained using the microfluidic assay device are in agreement with results obtained previously with traditional assays (15, 35).

Materials and Methods

Fluid Dynamics in Microdevices and Forces on Adherent Cells

To design and characterize the microfluidic devices of interest, we first used the simple Poiseuille model to explore the design space and determine the experimental regimes. This model assumes parallel plate configuration with infinite aspect ratio in the cross sectional dimensions (see Fig. 1B). The shear stress (τ) and pressure drop (ΔP) are functions of

volumetric flow rate (Q), channel dimensions (height (h), width (w), and length (L)), and fluid viscosity (μ), as follows,

$$\tau = -\frac{6Q\mu}{h^2 w}$$

$$\frac{\Delta P}{L} = -\frac{6Q\mu}{h^3 w}$$

Calculation of the Reynolds number $\mathrm{Re} = \frac{uh\rho}{\mu}$ allowed determination of wall and entrance effects within the microchannels (where the average linear velocity (u) is calculated from the volumetric flow rate as $u = \frac{Q}{hw}$) (36).

Shear stresses and pressure drops were also calculated using the analytical solution for rectangular channel flow (37) to evaluate the accuracy of the simple Poiseuille model. The analytical expression represents the linear velocity (u) in terms of the spatial coordinates (x the length, y the height, and z the width)

$$u = -\frac{\Delta p}{2\mu l} y(y-h) + \sum_{m=1}^{\infty} \sin\left(\frac{m\pi y}{h}\right)\left(A_m \cosh\frac{m\pi z}{h} + B_m \sinh\frac{m\pi z}{h}\right) \qquad (3)$$

where

$$A_m = \frac{h^2 \Delta p}{\mu m^3 \pi^3 l}(\cos m\pi - 1), \quad B_m = -\frac{A_m(\cosh m\eta\pi - 1)}{\sinh m\eta\pi}, \text{ and } \eta = \frac{w}{h}$$

The shear stress at the wall is the derivative of u with respect to position y evaluated at $y = 0$, i.e.

$$\tau_w = -\mu\frac{du}{dy} = \mu\frac{\Delta p}{2\mu l}\left(\frac{1}{2}y - h\right) - \mu\sum_{m=1}^{\infty}\left(\frac{m\pi}{h}\right)\cos\left(\frac{m\pi y}{h}\right)\left(A_m \cosh\frac{m\pi z}{h} + B_m \sinh\frac{m\pi z}{h}\right) \qquad (4)$$

The pressure drop is determined from the total flow rate (Q) by integrating the velocity expression with respect to y and z:

$$\frac{\Delta p}{l} = \frac{Q}{\frac{1}{24\mu}hw(h^2 + w^2) - \frac{8}{\pi^5\mu}\sum_{n=1}^{\infty}\frac{1}{(2n-1)^5}\left[h^4 \tanh\left(\frac{2n-1}{2h}\pi w\right) + w^4 \tanh\left(\frac{2n-1}{2w}\pi h\right)\right]} \qquad (5)$$

The infinite sums converged quickly, and were truncated when the convergence criteria

$$\frac{1}{(2N-1)^5}\left[h^4 \tanh\left(\frac{2N-1}{2h}\pi w\right)+w^4 \tanh\left(\frac{2N-1}{2w}\pi h\right)\right]$$
$$<\sum_{n=1}^{N-1}\frac{1}{(2n-1)^5}\left[h^4 \tanh\left(\frac{2n-1}{2h}\pi w\right)+w^4 \tanh\left(\frac{2n-1}{2w}\pi h\right)\right] \quad (6)$$

was satisfied.

Computational Fluid Dynamic software (CFD-ACE+, Huntsville, AL) was used to evaluate flow and shear fields for cases with cells adhering to the bottom channel wall. Three-dimensional (3-D) models were constructed to emulate either a flat cell or a dome-shaped cell in order to understand the influence of wall topology (due to the presence of adherent cells) in shear stress determination (see Fig. 1A). We took a single-cell-domain approach, where half of a biological cell is placed inside a calculation domain (Fig. 1B). Experimental observations were used as guidelines for determining cellular parameters for this model. Specifically, the fibroblast cells used in this study were observed to be approximately 11 μm in diameter in suspension and spread to ~20 μm in diameter shortly after attachment. If each spread cell is modeled as a dome, the radius of curvature and the height of the dome can be calculated by assuming conservation of the cell volume. Thus, a dome height of 4 μm was used in our simulations (Fig. 1B). The calculation domain is 60 μm long, 30 μm wide, and 25 μm high, and the half-cell is placed at the right wall of the domain. The boundary conditions include non-slip at the top and bottom surface, symmetry at the left and right boundary (we assume there is a cell exactly mirroring the cell in the calculation domain to the left, and the cell is symmetric itself), and defined velocity (parabolic) at the inlet and open outlet. The width of the calculation domain also bears a physical significance; it is half of center-to-center distance between two attached cells, and therefore reflects the cell seeding density in the channel. The mesh generated for the computation is denser near the wall than towards the center of the channel because the velocity changes most rapidly near the wall and velocity profile near the wall is critical for the shear stress calculation. We estimated that with the mesh edge size we use (< 0.5 μm), the error in shear calculation is < 2%. Smaller mesh size only improves the accuracy incrementally but is more costly, and therefore were not used for most calculations. In each simulation, the pressure drop in the channel, shear stress on the cell, and the pressure on the cell were calculated.

Fabrication of Microfluidic Adhesion Devices

The microfluidic devices were fabricated using PDMS rapid prototyping technique (17). Briefly, the photolithography masks were drawn using Freehand 9.0 (Macromedia Inc., San Francisco, CA), and printed on emulsion films with 5080 dpi resolution. The masters were created using a photo-patternable epoxy (SU-8-50, Microchem Inc., Newton, MA) on silicon wafers using UV photolithography, and the PDMS elastomer devices were molded from the masters using 2-part Sylgard 184 silicone elastomer (Dow Corning, Midland, MI). For the two-layer long-term culturing devices, a first layer of SU-8 was spun, patterned using photolithography, developed only in the alignment mark areas, and cured on the silicon wafer before a second layer was spun, aligned and patterned. The two layers were subsequently baked and developed simultaneously. The masters were silanized using vapor phase tridecafluoro-1,1,2,2-tetrahydrooctyl trichlorosilane (United Chemical Technologies, Bristol, PA) under vacuum before the PDMS was cured on them. The details of this process are shown in Fig. 2. Once cured, the devices were cut out, fluid access holes drilled, device bonded to glass slides by using oxygen plasma treatment of the PDMS prior to bonding, and tubing attached. A second layer of PDMS was usually cast over the bonded devices and treated at 60 °C for 2 hr to reinforce the mechanical stiffness of the PDMS device. These devices are then ready for the substrate coating and subsequent experiments.

Cell Cultures

The fibroblast cell line WT NR6, a 3T3 variant that lacks endogenous EGF receptor (EGFR) but that expresses stably-transfected human EGFR (38, 39), was routinely cultured in minimum essential medium-α (MEMα) supplemented with 7.5% fetal bovine serum (FBS), 350 _g/mL G418, 1 mM sodium pyruvate, 2 mM L-glutamine, 1 mM non-essential amino acids, 100 i.u./mL penicillin, and 200 _g/mL streptomycin. Adhesion assay medium comprised MEMα with 25 mM HEPES supplemented with 1% dialyzed FBS and 1 mg/mL bovine serum albumin (BSA), with or without 100 nM EGF.

Adhesion Assay

Prior to the assay, the microfluidic channels were sterilized with 70% ethanol and rinsed thoroughly with phosphate buffered saline (PBS). Channels were then flushed with excess

volumes of human plasma fibronectin (Gibco BRL) diluted in PBS (calcium- and magnesium-free), followed by physical adsorption of fibronectin onto the channel surfaces under static conditions for 1 hour at room temperature. After rinsing with PBS, channel surfaces were incubated with 2% BSA for 1 hour at room temperature to block nonspecific protein adsorption. All substrates were kept under PBS until cell seeding. WT NR6 cells were harvested using Versene (0.2% EDTA) to maintain integrin adhesion receptor integrity. In the short-term assays, cells were allowed to attach inside the microfluidic channel for 30 minutes at 37 °C in HEPES assay medium. Cell detachment was dynamically captured using time-lapse videomicroscopy. Briefly, a device seeded with cells was placed on a Ludl 99S008 motorized stage on a Zeiss Axiovert 35 microscope. Three to four fields were selected from each channel (typically 30-150 cells per field) and images were acquired every 2 minutes using the OpenLab software (Improvision Inc., Boston, MA). Because divalent cations are required for integrin-ligand binding, the shear buffer tubing was connected to a syringe filled with PBS that contained calcium and magnesium. Buffer flow rate was controlled using a Harvard Apparatus syringe pump (PH2000). Each experiment was repeated two to four times. The error bars represent the standard deviation of measurements obtained from separate experiments. Cell detachment was quantified post-assay. The fraction of adherent cells was determined for each channel as the number of cells remaining adherent at a given time divided by the initial number of cells when no flow was applied. In the long-term assays, the device was turned upside-down immediately after seeding to allow cells to sediment and attach to the protein-coated (3 _g/mL fibronectin) PDMS surface, without entering the side perfusion channels, to minimize obstruction of the flow. Cells were incubated in HEPES assay medium for 1-2 hours post-seeding prior to perfusion to allow cell attachment. Medium was then delivered to the device via the top perfusion chamber route at a rate of 2 _L/min for 10 hours using a syringe pump. Cells were subsequently incubated in assay medium with or without 100 nM EGF for 1 hour. The adhesion assay was conducted as described previously.

Results and Discussion

Device Design and Fabrication

The design of the microfluidic cell adhesion devices was motivated by the following experimental objectives: systematic variation in ligand-receptor interactions, systematic variation

in shear stress, study of short-term (<2 hr) as well as long-term (> 12 hr) adhesions, and all these in the context of high-throughput assay performance. The designs exploit the available microfabrication techniques and advantages of the microfluidic systems. In these micro-flow systems, viscous effects dominate, and pressure forces are not significant in most cases, except at high flow rates.

The device design was guided by both analytical and numerical solutions of the laminar flow problems in confined channels. Fig. 3A compares the different values of shear stress as a function of flow rate derived from the simple planar Poiseuille model to those of the 3-D analytical solutions for rectangular pipe flow. These calculations were done for a channel that is 25 μm thick and 250 μm wide (i.e. aspect ratio of 10). This constitutes a worst-case scenario, since all experiments were done in channels with an aspect ratio greater than 10. To a first order approximation, the simple model captures the shear stress characteristics in these microfluidic systems.

Both the analytical and numerical calculations demonstrate that more than 90% of the channel experiences a uniform shear stress distribution in the y direction (Fig. 3B), consistent with the general observation that the wall effect persists within one height from the sidewall (36). Therefore, in the designs with high aspect ratio, most of the cells are subject to a uniform shear stress. Accordingly, cells residing in the 5% edge area from each side of the channel are disregarded during post-assay counting. Another related design requirement is having fully developed flow under experimental conditions. The entrance length, i.e. the length it takes for the flow to become fully developed is a function of the Reynolds number (*Re*): the larger *Re* the longer the entrance region. For our experimental conditions, *Re* spanned from unity to a few hundred, depending on the flow rate (36). Nevertheless, rule of thumb estimates as well as the above-mentioned numerical calculation of flow in empty channels show that the entrance length is less than 1 mm, which is small compared to the length of the channel (10-20 mm). In the experiments, the entrance regions of the channel were excluded during image acquisition.

In the design, we also considered the effect of cell topology. Olivier et al. and Gaver et al. among others have examined how the presence of cell in the flow field influences the forces

exerted on the cell in Stokes flow (40-42). Although the flows in this work are laminar, the Reynolds numbers are sufficiently large so that the Stokes flow approximation ($Re < 0.1$) is not appropriate. Nevertheless physical insights from the abovementioned work remain useful in drawing intuitive conclusions on forces acting on the cells. Gaver and Kute concluded that in micro-scale when the ratio of cell dimension to channel dimension is not low, the actual shear stress felt by the cells could be significantly different from the wall shear stress in micro-scale because of a non-negligible distortion of the flow by the physical presence of the cell. Because the force calculation seems to be highly sensitive to the actual geometry, we have employed 3-D numerical simulations to compute the shear force on the cell surface as well as the pressure force on the body of a dome-shaped cell. The presence of a non-flat cell in the micro-channel changes the velocity distribution and correspondingly the shear stress distribution (Fig. 4A). Not surprisingly, the top of the cell dome experiences higher shear stresses than the edge of the cell. We found, however, that while the average shear stress the cell experiences is comparable to the shear stress corresponding to an empty channel, there is a significant pressure force acting on the cell in the direction of the flow (Fig. 4B). This pressure effect is sensitive to Re (flow rate) because the distortion in the velocity field gives rise to the drag force and the flow is no longer unidirectional. These observations are in agreement with the conclusion drawn from Kute's studies.

The present simulations do not capture the dynamic changes in cell shape. In principle, more information on the exact shape and dimensions of the cells can be extracted from microscopy images at any given time during the experiments and then used as input to the calculations of the force experienced by the cells. Olivier et al. in 1993 presented an interpretation of the shear response as a representation of the adhesion bond strength, number, and equilibrium constants (41). The same group later used AFM techniques to track the changes of cell shape and localization of adhesion forces (40). It is conceivable that by incorporating the image analysis information this type of shear assay could be standardized and become more quantitative on single cell level. It would also be possible to use more detailed mechanical models for cells under distractive forces, such as the peeling model or the bell model (43-48). Nonetheless, we envision that many of the applications of this assay will be comparative studies where the average force required to detach cells in the population will be used as a metric to rank the

effects of adhesion ligands or soluble adhesion mediators, and for such comparative assays the calculations provided here are sufficient.

Using these calculations and models as guidelines, we have designed two sets of short-term devices (Figs. 5A and 5B) – the multi-sample device which accommodates different substratum materials or cell types, and the multi-shear device which provides multiple platforms for different shear stresses. Lastly, we considered nutrient and exogenous reagent delivery for longer-term cell incubation. Unlike the short-term assays, nutrient depletion becomes a critical issue in experiments that require long-term cell culture. To provide continuous medium perfusion, a two-layer device was designed in which the nutrients can be delivered through a bifurcated side-channel network (Fig. 5C). Such a flow distribution scheme minimizes the subsequent shear stress experienced by the cells during delivery and ensures uniform delivery along the main channel. We estimated that the shear stress the cells experience during perfusion under such experimental conditions is physiologically insignificant (< 0.05 dynes/cm^2). To address material delivery and exchange, it was estimated that by diffusion alone, the mass transfer time scale from the top of the channel to the bottom (25 μm) is ~ 1-10 sec (using 10^{-9} - 10^{-11} m^2/sec as an estimate of the diffusion coefficient). Fluid convection further enhances mass transfer. Therefore, compared to the average fluid residence time in the micro channel (~1 min), the mass-transfer time scale is sufficient for satisfactory material exchange between the cells and the fresh medium. Other additional advantages of the two-layered design include the following: (1) the small thickness (3 μm) of the perfusion network prevents the cells from entering the side channels, thereby minimizing flow obstruction arising from cells and debris; (2) the flow provides adequate gas exchange and minimizes the probability of bubble formation; (3) the perfusion network can also be used to deliver exogenous reagents such as cell stimulants, inhibitors, and toxins.

Cell Adhesion on Varying Protein-coated Surfaces

Cell attachment to a substrate is established through interactions between cell surface adhesion receptors and various extracellular-matrix (ECM) adhesion ligands. It is well established that cell adhesion strength is a function of the number and the specificity of the receptor-ligand complexes formed. The multi-sample microfluidic device has channels that

allow multiple conditions to be examined in one experiment. This high-throughput design minimizes time, reagents, and inter-experimental variations. The identical dimensions of each channel on a single device as well as the fidelity of channel dimensions from device to device ensure that the same shear stress is maintained in all channels. In this way, the measured adhesion difference can be attributed solely to systematic variations in ligand-receptor interactions.

Fibronectin was used as a prototype ECM protein. Each of the four channels was coated with fibronectin molecules from solutions of 0, 0.1, 1, and 10 μg/mL, respectively. By introducing step increases in the shearing buffer flow rate at discrete time intervals, shear stress was increased from 0 to 1,600 dynes/cm^2 with time throughout the assay to sample increasing levels of shear-force response. Cell adhesion strength depended on fibronectin surface density (Fig. 6). At the highest fibronectin density (corresponding to a coating concentration of 10 _g/mL of fibronectin), barely 10% of the cells seeded in the channel were detached at the end of the experiment. In contrast, at the lowest ligand density (0.1 _g/mL coating density), nearly all cells were removed shortly after a small shear force was introduced. As expected, at the intermediate coating concentration (1 _g/mL), cells exhibited a gradual detachment profile as the shear stress was increased. Such dependence of WT NR6 adhesion strength on fibronectin surface density has been observed before using the centrifugation assay (16). However, the fibronectin coating concentrations sampled were usually limited to less than 1 _g/mL in order for the cells to be susceptible to the detachment forces allowed by the centrifuge. This multi-sample device has been also used to measure and compare the adhesion strength of a parental cell line and its cytoskeletal mutants (data not shown). These experiments clearly demonstrate that the microfluidic adhesion device can be used to probe cell adhesive response to ECM ligand concentration in a high-throughput format. Furthermore, the force range (0 - 1,600 dynes/cm^2) used in the experiment is well within the capability of our device. We describe in the subsequent sections that the microfluidic devices can detach cells at higher fibronectin density (e.g. 10 _g/mL) and after they have been cultured overnight.

Cell Adhesion with Varying Shear Stresses

There are many instances where the measurement of interest is the dynamic biophysical response of cells to different external forces. In the previous experiment, shear stress was varied during the assay by varying the buffer flow rate. However, this protocol may introduce complications in quantitative interpretation of the results when force response is of interest, since the effects of time and force are convoluted. Therefore, the next design objective is to create an array of channels that offer different values of time-invariant shear stress in a high-throughput fashion. In conventional approaches such as centrifugation or parallel plate assay, it is not possible to sample more than one force at a time. The radial flow assay and the parallel plate assay with tapered channels allow simultaneous sampling of different force conditions, but the continuous change in geometry complicates exact force determination, and minute variations in chamber height as a result of device assembly makes it difficult to maintain experimental reproducibility. In our study, the multi-shear device achieves built-in variation in shear stress across the channels by giving each channel a different width while maintaining identical pressure drop by compensating with the length of the channels. For example, when channel width is narrowed from 1000 μm to 750 μm and to 500 μm, the length is shortened accordingly, and a 1.5-fold and 2-fold increase in shear stress, respectively, is effectively introduced. During the experiments, samples were taken from different channel locations, therefore minimizing errors arising from other experimental factors such as non-uniform seeding density.

Previous experiments using the multi-sample device showed strong cell adhesion on a 500 μm wide channel coated with 10 _g/mL of fibronectin, with only ~10% of cells distracted at the maximal shear stress value of 1600 dyne/cm^2. To capture the dynamic cell detachment profile effectively, much higher shear stress must be applied. Therefore a constant flow rate of 1.25 mL/min per channel was selected and applied throughout the experiment using the multi-shear device to maintain time-invariant, but channel width-dependent, shear stress in channels with 500, 750, and 1000 μm in width, yielding shear stress values of 4000, 2700, and 2000 dyne/cm^2, respectively. With these relatively high levels of shear stress, different cell adhesion profiles were obtained in the high adhesion regime (10 _g/mL of fibronectin), as illustrated in Fig. 7. At a shear stress level of 2000 dynes/cm^2 applied for 12 minutes, only ~10% of the cells detached, but at a 2-fold higher level of shear stress, greater than 90% of the cells came off the surface in the same time period. An intermediate adhesion profile was

obtained at an intermediate shear stress. The detachment profiles (Fig. 7) suggest that cell detachment is a threshold phenomenon, occurring around 2500-3500 dyne/cm^2. Additionally the linear detachment profile suggests that 2700 dynes/cm^2 is a force regime to which most of the cell population is susceptible; therefore it provides the most dynamic detachment kinetics under the given conditions. On the other hand, cell response obtained from the 500 μm-wide channel showed that 80% of the cells came off the substrate within the first 4 minutes when the shear stress is further increased to 4,000 dynes/cm^2. Therefore this force regime captures only the detachment dynamics of a small and highly adhesive population of the cell adhesion histogram. In one experiment, the multi-shear device can effectively identify the force-response regimes of a cell population of interest. This device thus provides a platform to study the kinetics and mechanism of cell detachment from the substrates. Moreover, it can be used in higher magnification microscopy mode to capture the dynamic changes in cell contour, which would facilitate the formulation of shape-dependent models of cell adhesion.

In this set of experiments, we have shown that the multi-shear device provided a systematic approach to varying shear stress, determining the force level that is most relevant for the adhesion measurement of a cell population of interest, as well as performing the kinetics study of these population events. These designs can be further integrated into one device to enable combined high-throughput testing of materials under different shear conditions.

Long Term Shear Assays – Nutrient and Reagent Delivery

Long-term cell adhesion is rarely quantified, in part because force of large magnitude is required to detach well-adherent cells such as fibroblasts. For example, using a spinning disk device, Garcia et al. demonstrated a 10-20 times increase in adhesion strength after IMR-90 fibroblasts were plated overnight on surfaces coated with 2 _g/mL of fibronectin, which required a shear stress as high as 2500 dynes/cm^2 (after adding 50 mg/mL dextran to shearing buffer to increase buffer viscosity) for cell removal (28). A conventional parallel plate device has typical dimensions on the order of 1mm x 1mm (width by height), which will require unrealistically high flow rates in order to generate forces strong enough to remove adherent cells. It is also reported elsewhere that only 30% of adherent fibroblast cells are detached at ~59,000g using an ultracentrifuge (29). The force range is usually between 1g and 4,500g in most commercial

super-centrifuges that can be adapted to cell adhesion assays. In the previous two sections, we described how the values of shear stress achievable in microchannels overcome such limitations. Long-term incubation in micro devices, however, is still a challenge due to issues such as nutrient delivery and bubble generation.

A typical microfluidic channel holds a total volume on the order of a microliter. Thus nutrient delivery and medium exchange is critical in maintaining long-term cell viability. For example, oxygen consumption rates for mammalian cells vary between 0.05 and 0.5 pmol/cell/hr (49). Given an estimated oxygen solubility of 2×10^{-4} _mole/mm^3 in cultured medium at 37 °C, oxygen becomes limiting within an hour of incubation in the micro-device. As illustrated in Fig. 8A, when cells were incubated in the long-term device for 12 hours without perfusion on 10 _g/mL fibronectin, many of the cells rounded up or had fragmented cell membranes, indicative of unhealthy or dying cells. Similarly, growth factors with estimated consumption rate ~3 amol/cell/hr (assuming negligible ligand depletion and recycling, with 100,000 EGFR/cell, and an internalization rate constant of 0.3 min^{-1} (51)) could also become limiting. In addition to the material exchange concern, it is conceivable that nucleation of gas bubbles is more facile in micro-devices because of the large surface area-to-volume ratio and the accumulation of cellular debris. To address these issues, a dual-chamber perfusion design is introduced to allow cell adhesion quantification after overnight incubation, and to improve nutrient and gas exchange within the micro-channels. These perfusion networks can also be used to deliver exogenous reagents uniformly throughout the channel, thereby allowing biochemical studies to be performed. Moreover, the shear stress introduced during medium delivery from the bifurcated channels is minimal. The dual-chamber design also prevents cells from moving into the bifurcated network and interfering with the fluid distribution. When fresh assay medium was delivered at a rate of 2 _L/min, cells continued to spread and retained an appearance that is similar to those cultured under macroscopic conditions (Fig. 8B), and no bubble generation was observed under the flow conditions.

Cell adhesion is regulated not only through adhesion to the matrix proteins, but also by soluble molecules. For example, EGF has an established role in disassembly of focal adhesions, thereby reducing cell adhesion and in many cases enhancing cell motility (15, 35, 52). Typical protocols adopted to study EGF effects usually involve an extended period of growth factor-

deprivation to return EGF signaling to basal level, which is then followed by EGF stimulation. Using the perfusion device, WTNR6 fibroblasts were serum-starved for 12 hours inside channels coated with 3 _g/mL of fibronectin. The perfusion chamber then uniformly delivered EGF to sample channels. After 1 hour of treatment, the adhesion assay was performed to assess cell response. The weakening effect of EGF on cell adhesion is clearly demonstrated in Fig. 9. The majority of the treated cells were removed after a shear stress of 6400 dynes/cm^2 was applied for 3 minutes, while the control population exhibited higher resistance to shear, 10% of which remained attached after the same stress was applied for 9 min. It should be noted that we were able to remove fully spread fibroblasts at the end of the assay by applying ~6000 dynes/cm^2, using a flow rate that is well within the technical limit of the system. This threshold of detachment force is comparable to the 2500 dynes/cm^2 shear stress reported by Garcia et al. using the IMR-90 fibroblasts (28), and is in agreement with the theoretical calculation of ~6000 dynes/cm^2 by Olivier et al (41). Furthermore, the results also demonstrate the importance of employing quantitative methodology in addressing biological phenomena. More specifically in our experiments, without knowing the relevant detachment force range for the cell population of interest, the adhesion strength of EGF-treated and untreated cells appeared to be similar when only a small shear stress was applied. However, this is misleading since 1500 dynes/cm^2 was apparently below the threshold force for either cell samples to be detached. At a higher shear stress, the difference between the treated and control populations became evident.

In these experiments, we have successfully cultured cells for the study of long-term biochemical and biomechanical effects on cell adhesion in micro-channels. The microfluidic assays properly identified the appropriate detachment force range and clearly demonstrated the de-adhesive effects of EGF that has been observed using conventional methods (15, 35). Furthermore, the assay achieved adequate shear stress to remove fully spread cells. It is conceivable that these devices can be incorporated as an upstream component to other micro-devices that perform molecular analysis (53). Once integrated, these systems would have the potential to facilitate high-throughput analysis of many types of biologically phenomena, such as mechanotransduction.

Conclusion

Exploiting the unique fluidic properties of micro-scale flow, we demonstrated high-throughput experimentation on cell adhesion using microfluidic devices. The multi-sample and multi-shear devices are representative of the prototype designs used to demonstrate and validate the working principle of microfluidic cell adhesion assays. Because of the small dimensions, we are able to achieve large shear stress using small fluid flow and perform the assays with small volume of reagents and shearing fluids on a small number of cells. Through design manipulations studies of time-dependent and soluble-factor-dependent cell adhesion phenomena were also made possible. High-throughput testing and the amendable design of these devices would allow efficient assessment of a plethora of regulative mechanisms for cell adhesion by introducing multiple changes to the extracellular environment in one experiment. The applications of such devices can be broadened to other cell-based biological assays, such as cell migration. Finally, it has the potential to be incorporated into an integrated micro Total Analysis Systems (μTAS) (54, 55) as an upstream unit followed by downstream separation and detection micro-units for fast and high-throughput elucidation of molecular mechanisms underlying cell adhesion.

Acknowledgments

We thank the DARPA Bio-Info-Micro Program (MDA972-00-1-0030), the NIH Cell Migration Consortium (NIH GC10641), the NSF graduate fellowship to HL, and the Whitaker Foundation graduate fellowship to LYK for financial support, and the technical staff of the Microsystems Technology Laboratories at MIT for technical assistance.

References

1. Burmeister, J. S., Vrany, J. D., Reichert, W. M. & Truskey, G. A. (1996) *Journal of Biomedical Materials Research* **30,** 13-22.
2. Tempelman, L. A. & Hammer, D. A. (1994) *Biophysical Journal* **66,** 1231-1243.
3. Vankooten, T. G., Schakenraad, J. M., Vandermei, H. C. & Busscher, H. J. (1992) *Journal of Biomedical Materials Research* **26,** 725-738.
4. Cozensroberts, C., Quinn, J. A. & Lauffenburger, D. A. (1990) *Biophysical Journal* **58,** 857-872.
5. Garcia, A. J., Ducheyne, P. & Boettiger, D. (1997) *Biomaterials* **18,** 1091-1098.
6. Powers, M. J., Rodriguez, R. E. & Griffith, L. G. (1997) *Biotechnology and Bioengineering* **53,** 415-426.
7. Usami, S., Chen, H. H., Zhao, Y. H., Chien, S. & Skalak, R. (1993) *Annals of Biomedical Engineering* **21,** 77-83.
8. McClay, D. R., Wessel, G. M. & Marchase, R. B. (1981) *Proceedings of the National Academy of Sciences of the United States of America-Biological Sciences* **78,** 4975-4979.
9. Hertl, W., Ramsey, W. S. & Nowlan, E. D. (1984) *In Vitro-Journal of the Tissue Culture Association* **20,** 796-801.
10. Chu, L., Tempelman, L. A., Miller, C. & Hammer, D. A. (1994) *AIChE Journal* **40,** 692-703.
11. Tozeren, A., Sung, K. L. P., Sung, L. A., Dustin, M. L., Chan, P. Y., Springer, T. A. & Chien, S. (1992) *Journal of Cell Biology* **116,** 997-1006.
12. Evans, E., Leung, A., Hammer, D. & Simon, S. (2001) *Proceedings of the National Academy of Sciences of the United States of America* **98,** 3784-3789.
13. Merkel, R., Nassoy, P., Leung, A., Ritchie, K. & Evans, E. (1999) *Nature* **397,** 50-53.
14. Athanasiou, K. A., Thoma, B. S., Lanctot, D. R., Shin, D., Agrawal, C. M. & LeBaron, R. G. (1999) *Biomaterials* **20,** 2405-2415.
15. Maheshwari, G., Wells, A., Griffith, L. G. & Lauffenburger, D. A. (1999) *Biophysical Journal* **76,** 2814-2823.
16. Koo, L. Y., Irvine, D. J., Mayes, A. M., Lauffenburger, D. A. & Griffith, L. G. (2002) *Journal of Cell Science* **115,** 1423-1433.
17. Duffy, D. C., McDonald, J. C., Schueller, O. J. A. & Whitesides, G. M. (1998) *Analytical Chemistry* **70,** 4974-4984.
18. Burns, M. A., Johnson, B. N., Brahmasandra, S. N., Handique, K., Webster, J. R., Krishnan, M., Sammarco, T. S., Man, P. M., Jones, D., Heldsinger, D., Mastrangelo, C. H. & Burke, D. T. (1998) *Science* **282,** 484-487.
19. Cheng, J., Sheldon, E. L., Wu, L., Uribe, A., Gerrue, L. O., Carrino, J., Heller, M. J. & O'Connell, J. P. (1998) *Nature Biotechnology* **16,** 541-546.
20. Fu, A. Y., Spence, C., Scherer, A., Arnold, F. H. & Quake, S. R. (1999) *Nature Biotechnology* **17,** 1109-1111.
21. Hatch, A., Kamholz, A. E., Hawkins, K. R., Munson, M. S., Schilling, E. A., Weigl, B. H. & Yager, P. (2001) *Nature Biotechnology* **19,** 461-465.
22. Santini, J. T., Cima, M. J. & Langer, R. (1999) *Nature* **397,** 335-338.
23. Voldman, J., Gray, M. L., Toner, M. & Schmidt, M. A. (2002) *Analytical Chemistry* **74,** 3984-3990.
24. Weigl, B. H. & Yager, P. (1999) *Science* **283,** 346-347.

25. Kenis, P. J. A., Ismagilov, R. F. & Whitesides, G. M. (1999) *Science* **285,** 83-85.
26. Lotz, M. M., Burdsal, C. A., Erickson, H. P. & McClay, D. R. (1989) *Journal of Cell Biology* **109,** 1795-1805.
27. Goldstein, A. S. & DiMilla, P. A. (1997) *Biotechnology and Bioengineering* **55,** 616-629.
28. Garcia, A. J., Takagi, J. & Boettiger, D. (1998) *Journal of Biological Chemistry* **273,** 34710-34715.
29. Rich, A. M. (1978) (University of North Carolina, Chapel Hill).
30. Abbasi, F., Mirzadeh, H. & Katbab, A. A. (2001) *Polymer International* **50,** 1279-1287.
31. Aucoin, L., Griffith, C. M., Pleizier, G., Deslandes, Y. & Sheardown, H. (2002) *Journal of Biomaterials Science-Polymer Edition* **13,** 447-462.
32. Eteshola, E. & Leckband, D. (2001) *Sensors and Actuators B-Chemical* **72,** 129-133.
33. Hu, S. W., Ren, X. Q., Bachman, M., Sims, C. E., Li, G. P. & Allbritton, N. (2002) *Analytical Chemistry* **74,** 4117-4123.
34. Xiao, D. Q., Zhang, H. & Wirth, M. (2002) *Langmuir* **18,** 9971-9976.
35. Xie, H., Pallero, M. A., Gupta, K., Chang, P., Ware, M. F., Witke, W., Kwiatkowski, D. J., Lauffenburger, D. A., Murphy-Ullrich, J. E. & Wells, A. (1998) *Journal of Cell Science* **111,** 615-624.
36. Deen, W. (1998) *Analysis of Transport Phenomena* (Oxford University Press, New York).
37. Happel, J. & Brenner, H. (1965) *Low Reynolds Number Hydrodynamcis with Special Applications to Particulate Media* (Prentice-Hall, Inc., Englewood Cliffs, N.J.).
38. Pruss, R. M. & Herschman, H. R. (1977) *Proceedings of the National Academy of Sciences of the United States of America* **74,** 3918-3921.
39. Chen, P., Gupta, K. & Wells, A. (1994) *Journal of Cell Biology* **124,** 547-555.
40. Olivier, L. A., Yen, J., Reichert, W. M. & Truskey, G. A. (1999) *Biotechnology Progress* **15,** 33-42.
41. Olivier, L. A. & Truskey, G. A. (1993) *Biotechnology and Bioengineering* **42,** 963-973.
42. Gaver, D. P. & Kute, S. M. (1998) *Biophysical Journal* **75,** 721-733.
43. Hammer, D. A. & Lauffenburger, D. A. (1987) *Biophysical Journal* **52,** 475-487.
44. Ward, M. D. & Hammer, D. A. (1993) *Biophysical Journal* **64,** 936-959.
45. Evans, E., Berk, D. & Leung, A. (1991) *Biophysical Journal* **59,** 838-848.
46. Evans, E., Berk, D., Leung, A. & Mohandas, N. (1991) *Biophysical Journal* **59,** 849-860.
47. Evans, E. A. (1985) *Biophysical Journal* **48,** 175-183.
48. Evans, E. A. (1985) *Biophysical Journal* **48,** 185-192.
49. Jorjani, P. & Ozturk, S. S. (1999) *Biotechnology and Bioengineering* **64,** 349-356.
50. Komarova, S. V., Ataullakhanov, F. I. & Globus, R. K. (2000) *American Journal of Physiology-Cell Physiology* **279,** C1220-C1229.
51. Lauffenburger, D. A. & Linderman, J. J. (1993) *Receptors* (Oxford University Press, New York).
52. Lu, Z. M., Jiang, G. Q., Blume-Jensen, P. & Hunter, T. (2001) *Molecular and Cellular Biology* **21,** 4016-4031.
53. Lu, H., Gaudet, S., Schmidt, M. A. & Jensen, K. F. (submitted).
54. Reyes, D. R., Iossifidis, D., Auroux, P. A. & Manz, A. (2002) *Analytical Chemistry* **74,** 2623-2636.
55. Auroux, P. A., Iossifidis, D., Reyes, D. R. & Manz, A. (2002) *Analytical Chemistry* **74,** 2637-2652.

Figure Legends

Figure 1. (A) General microfluidic device design for cell adhesion shear assays. The cells reside in a microfluidic channel that has large aspect ratio in cross-sectional dimensions (width-to-height). A non-flat cell experiences both shear forces, which act tangential to the cell surface, and pressure forces, which act normally on the protruding cell body in the flow field. Only in special cases (e.g. small fluid linear velocity, and very small cell height), the pressure force becomes negligible compared to the shear forces. (B) Dimensions of a computational domain used in the 3-D numerical model.

Figure 2. Fabrication processes used in the two-chamber perfusion micro device for long-term shear assays. The single layer devices (e.g. the short-term Multi-Sample and Multi-Shear devices) were fabricated using a similar process. (a) spin-coat the first thin layer with photo-patternable epoxy (SU-8); (b) pattern the SU-8 layer with photolithography; (c) soft-bake the SU-8 to complete the cross-linking process and develop the un-cross-linked SU-8 around the alignment mark area; (d) spin-coat the second layer of SU-8; (e) align and pattern the second layer of SU-8; (f) soft-bake the wafer; (g) develop both layers of SU-8; (h) silane-treat the SU-8 master to prevent sticking and micro-mold PDMS polymer on the SU-8 master; (i) bond the PDMS to glass slide and assemble fluid connections.

Figure 3. (A) Comparison between the simple planar Poiseuille flow model and the 3-D analytical solution to flow in rectangular pipes. The stress calculation derived from the planar model is a good approximation of the actual wall stress in a cell-free device in with large aspect ratio. (B) The stress distribution in the y-z cross-section of the microchannels. In the worst-case scenario with an aspect ratio of 10, over 90% of the channel wall experiences a uniform shear stress.

Figure 4. (A) Comparison between shear stress experienced by a protruding cell, calculated using the 3-D numerical model, and that experienced by a perfectly flat cell using the 3-D analytical solution. The average shear stress experienced by the cells remains essentially the same for cells with appreciable height compared to very flat cells. However, there is a significant pressure force component, as large as 30% of the shear force, acting on a protruding cell in the direction of the flow. (B) The 3-D numerical calculation also shows that (top) the apex of the cells experiences most of the shear forces while the basal areas near the bottom wall of the microchannels experience much less shear force; (bottom) the pressure forces acting in the direction of the flow pushes the cell at the rear end and pulling in the front end.

Figure 5. (A) Short-term adhesion Multi-Sample device accommodates one common inlet, which splits into 4 physically identical channels with separate inlets. (B) Short-term Multi-Shear device allows different time-invariant shear forces to be examined simultaneous while maintaining constancy in other conditions. (C) Long-term adhesion assay device has a two-layer design for uniform nutrient/reagents exchange

and delivery (see text). The bifurcation design ensures small shear stresses during fluid perfusion.

Figure 6. The effect of fibronectin coating concentration was studied using the Multi-Sample device. Short-term WT NR6 adhesion decreased dramatically in response to 10-fold and 100-fold reductions in fibronectin coating concentration. More cells were removed when shear stress was increased over time through increase in flow rate.

Figure 7. The effect of time-invariant shear stress was studied using the Multi-Shear device. WT NR6 cells in the 500 μm-wide channel experienced twice as much shear stress as those in the 1000 μm-wide channel, and were removed more readily. The intermediate stress applied through the 750 μm-wide channel detached cells at a linear rate that was intermediate of the other two channels.

Figure 8. (A) Without medium replenishment, WT NR6 cells did not survive a 12-hour incubation in the micro-channels. (B) With perfusion network to continuously deliver fresh medium, cell remained viable and healthy after a 15-hour culture in the long-term device.

Figure 9. After 12-hr of quiescence in the long-term device, WT NR6 cells treated with 100 nM of EGF, which was delivered using the perfusion network, exhibited markedly compromised adhesion compared to the untreated cells. While this difference was not apparent at 1500 dynes/cm^2, a shear stress at 6000 dynes/cm^2 revealed the effect of EGF and readily detached both cell populations.

Figure 1A

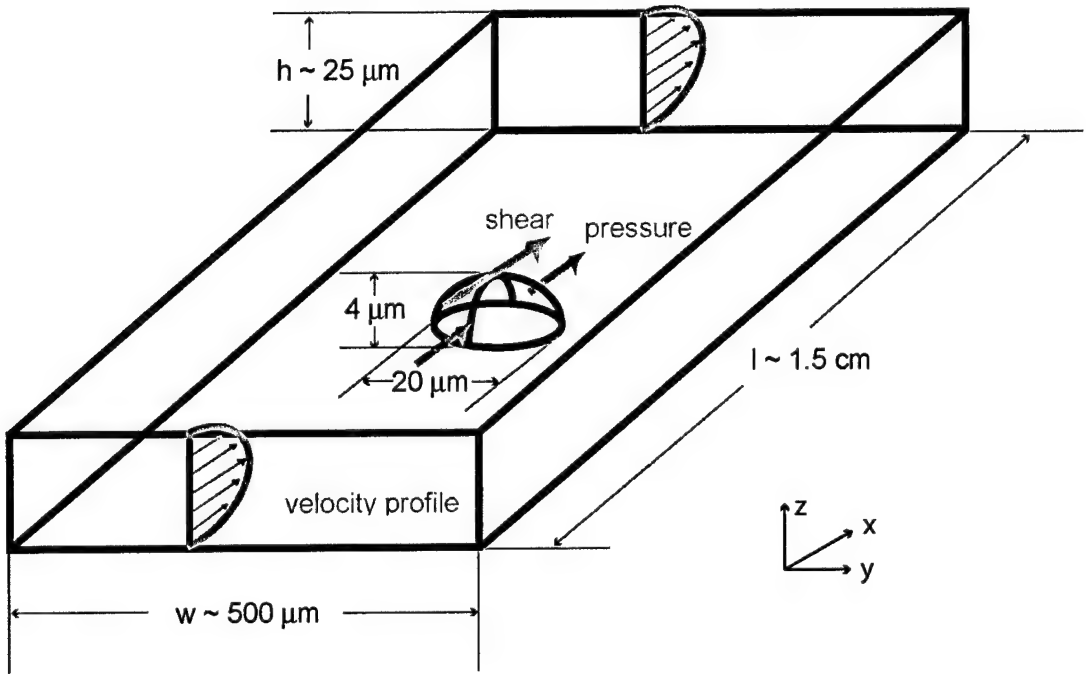
h ~ 25 µm
shear
pressure
4 µm
20 µm
l ~ 1.5 cm
velocity profile
z
x
y
w ~ 500 µm

Figure 1B

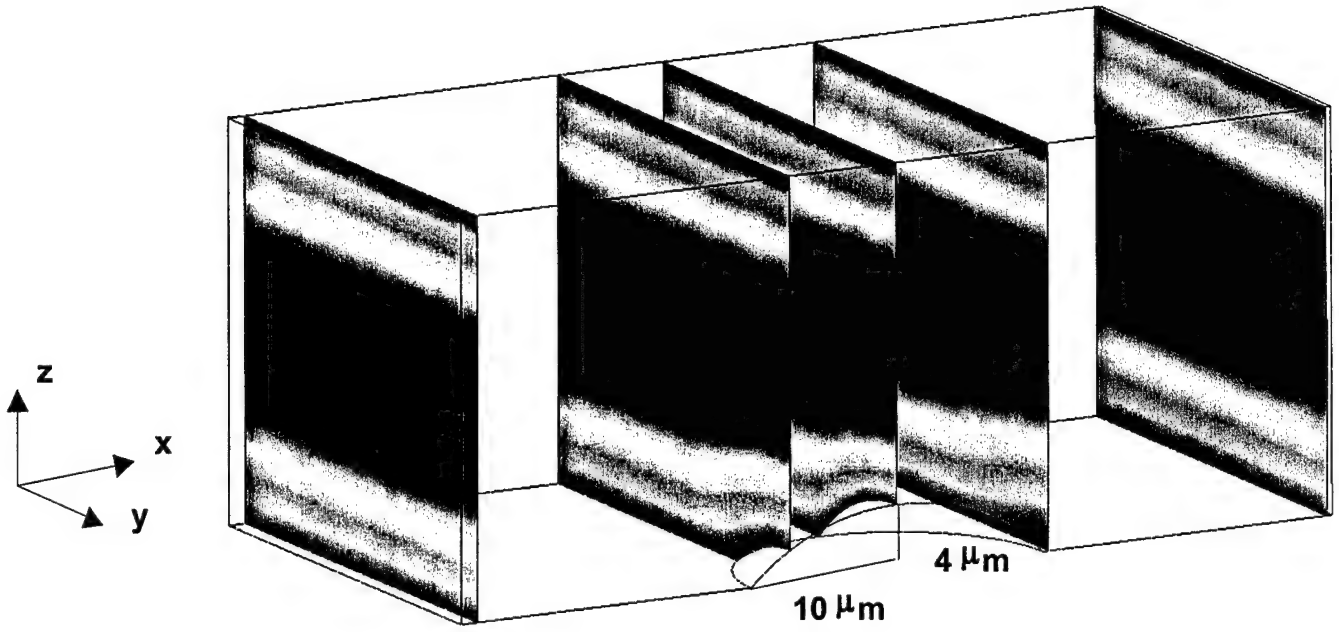

Figure 2

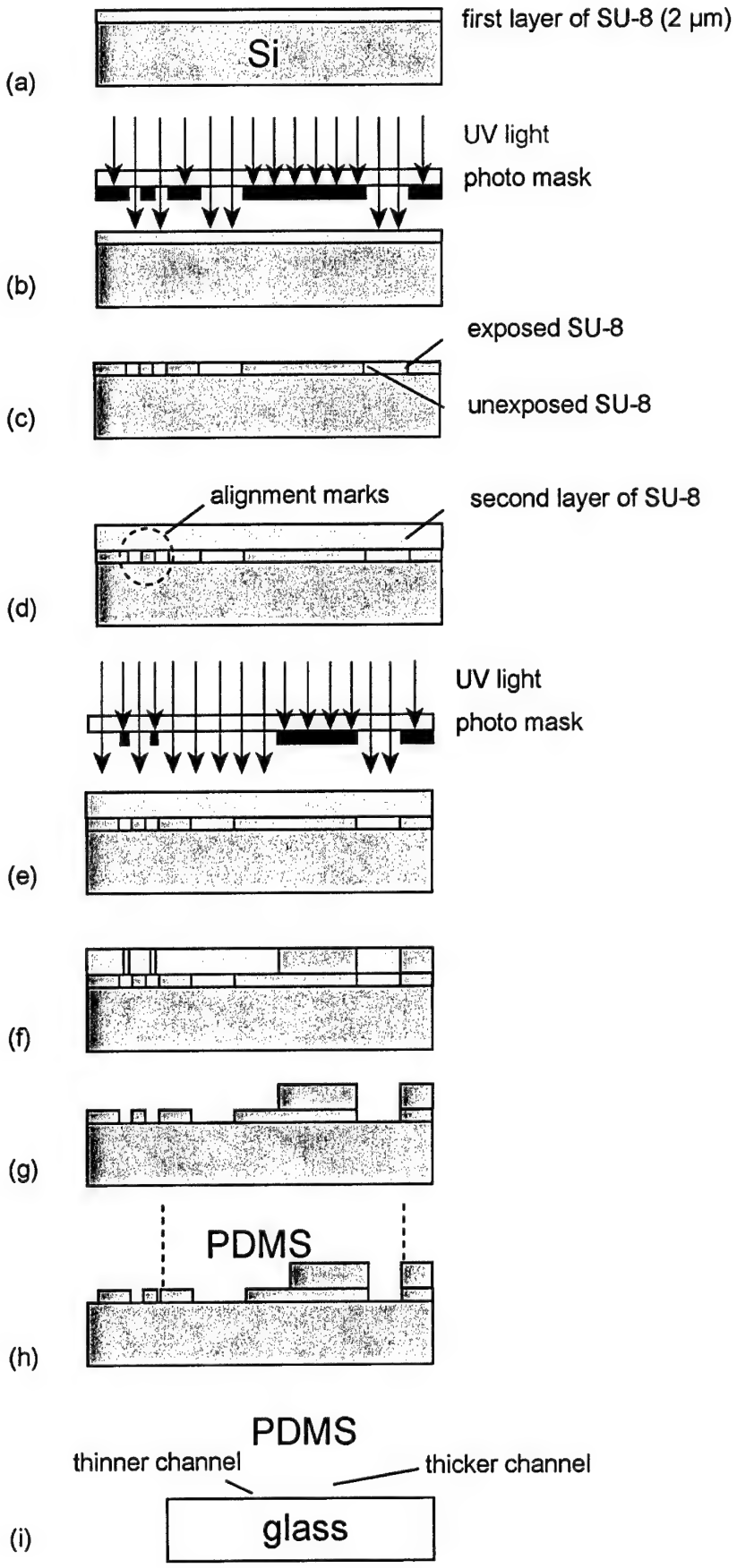
(a)
Si
first layer of SU-8 (2 µm)
(b)
UV light
photo mask
(c)
exposed SU-8
unexposed SU-8
(d)
alignment marks
second layer of SU-8
(e)
UV light
photo mask
(f)
(g)
(h)
PDMS
(i)
PDMS
thinner channel
thicker channel
glass

Figure 3A

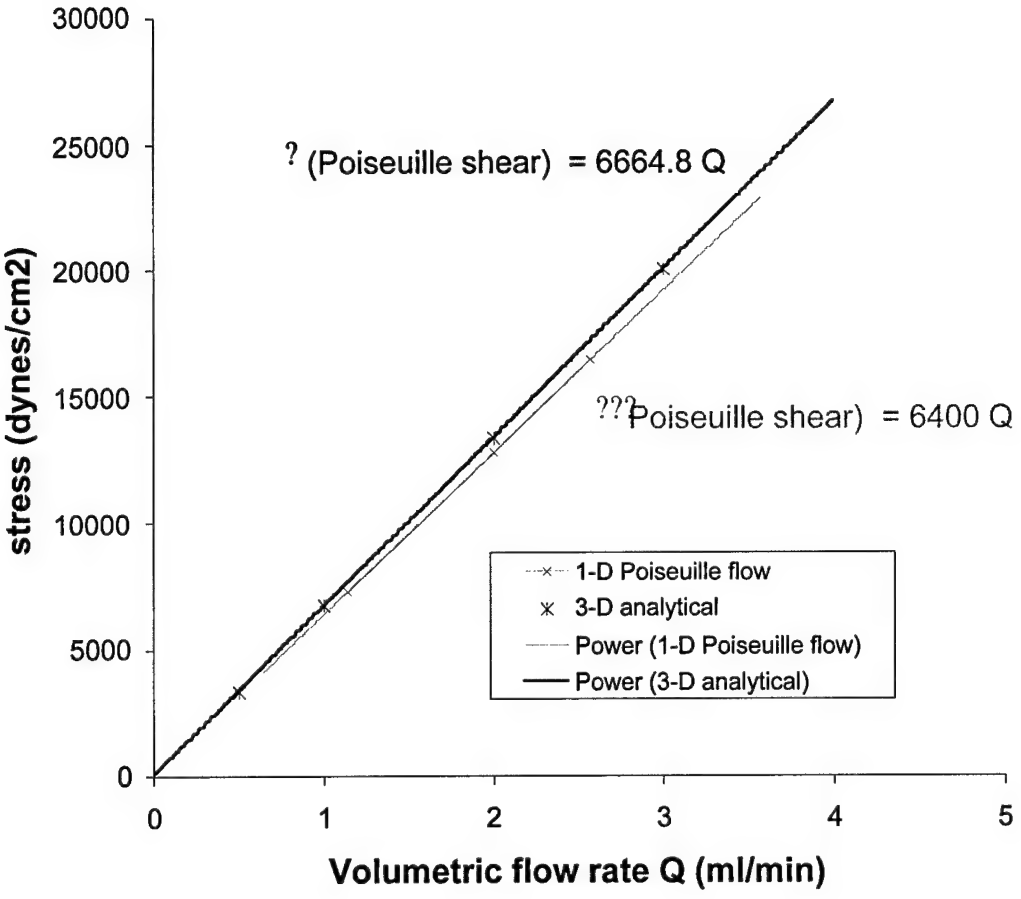
30000
25000
20000
15000
10000
5000
0
stress (dynes/cm2)
? (Poiseuille shear) = 6664.8 Q
??Poiseuille shear) = 6400 Q
1-D Poiseuille flow
3-D analytical
Power (1-D Poiseuille flow)
Power (3-D analytical)
0
1
2
3
4
5
Volumetric flow rate Q (ml/min)

Figure 3B

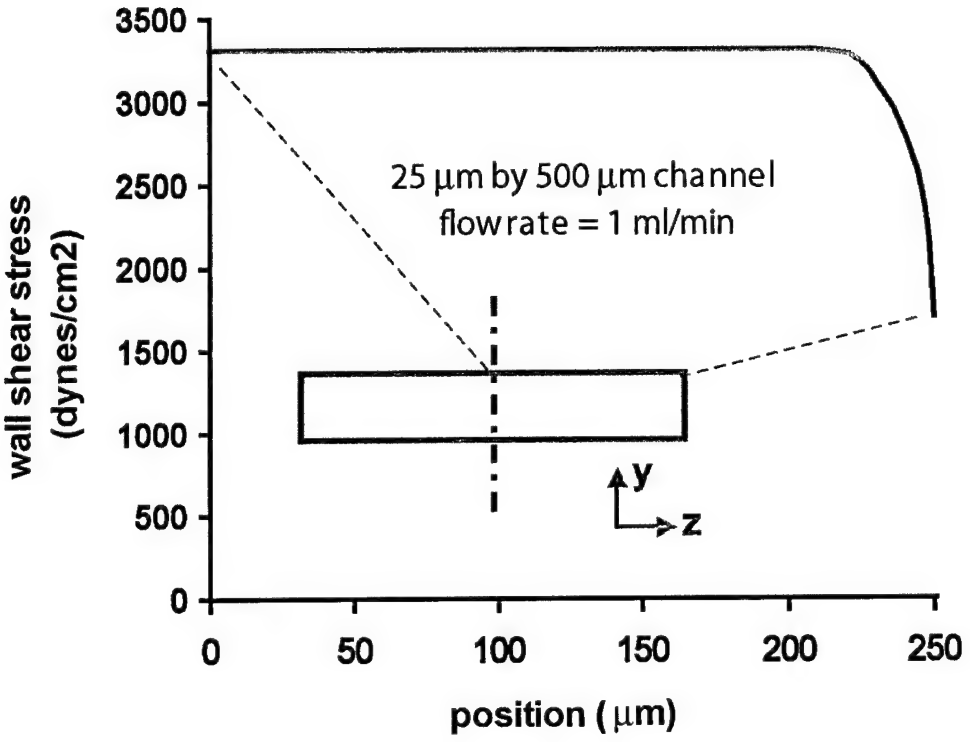
3500
3000
2500
2000
1500
1000
500
0
wall shear stress (dynes/cm2)
25 µm by 500 µm channel
flowrate = 1 ml/min
y
z
0
50
100
150
200
250
position (µm)

Figure 4A

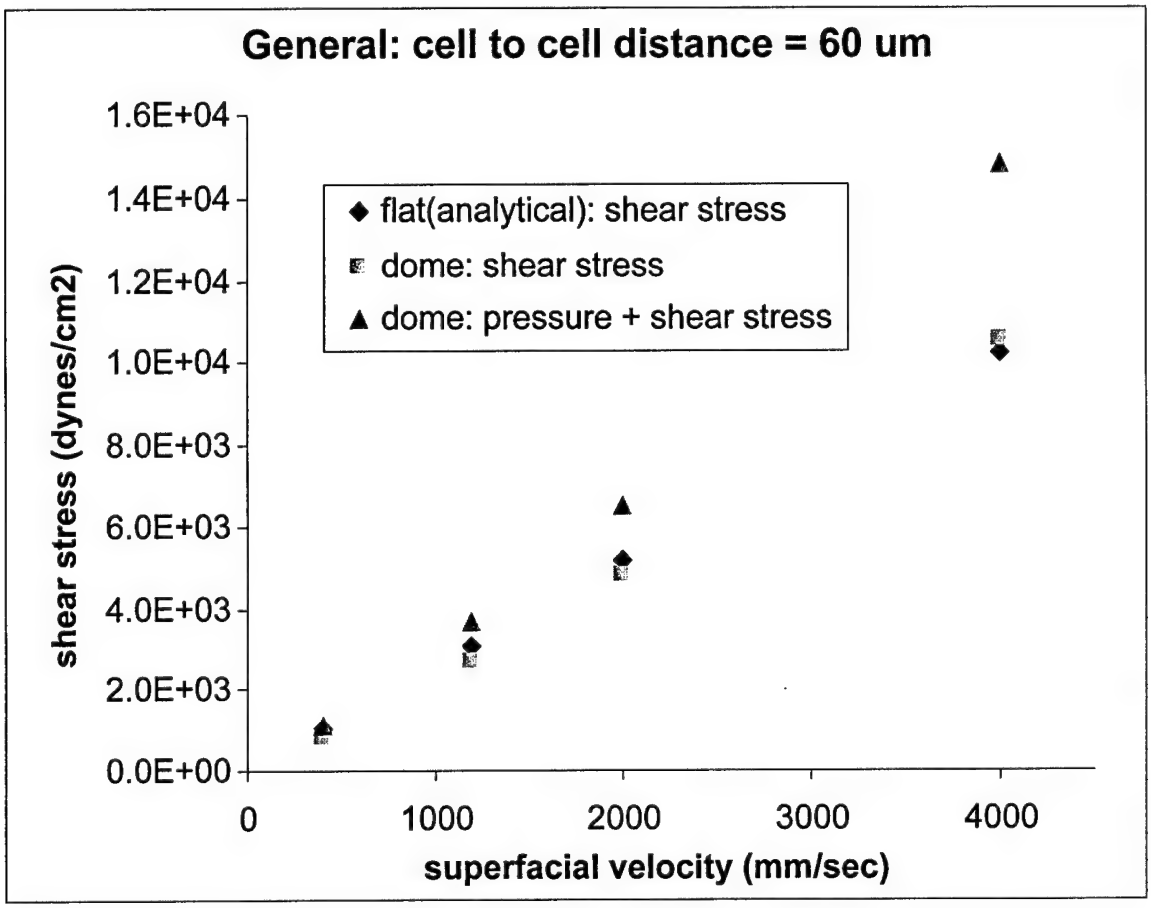
General: cell to cell distance = 60 um
1.6E+04
1.4E+04
1.2E+04
1.0E+04
8.0E+03
6.0E+03
4.0E+03
2.0E+03
0.0E+00
shear stress (dynes/cm2)
flat(analytical): shear stress
dome: shear stress
dome: pressure + shear stress
0
1000
2000
3000
4000
superfacial velocity (mm/sec)

Figure 4B

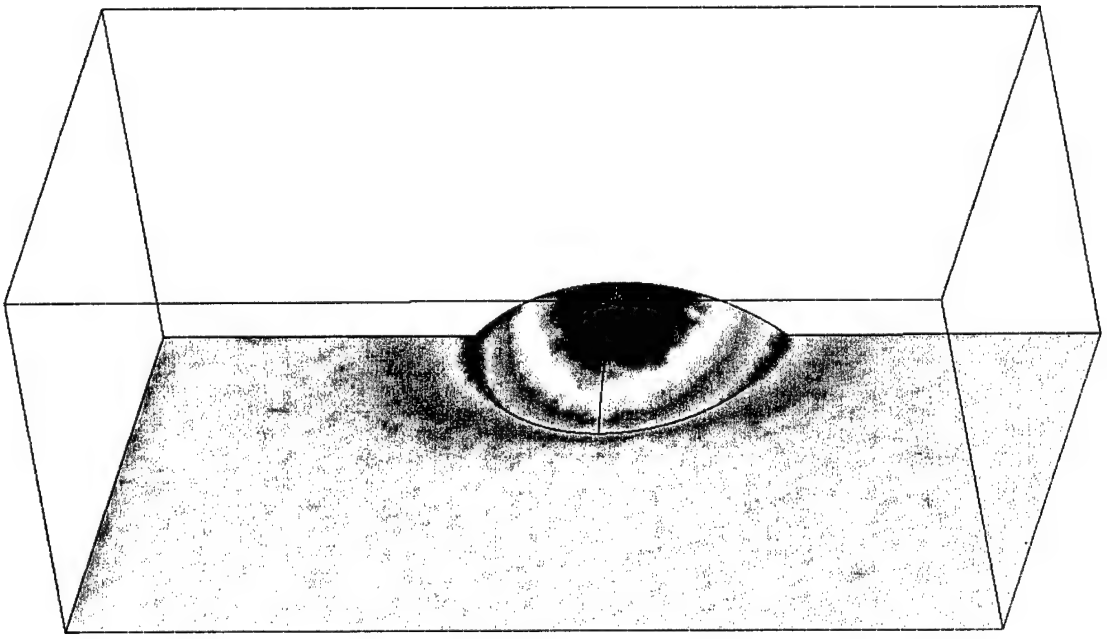

Figure 5A

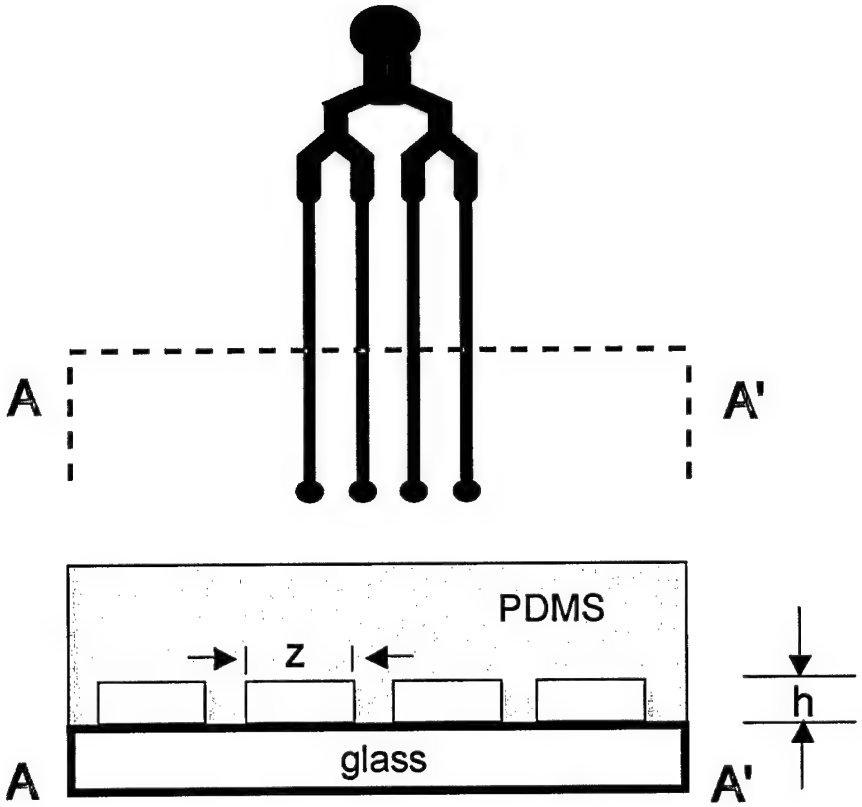

H =25 μm

z = 500 μm

Figure 5B

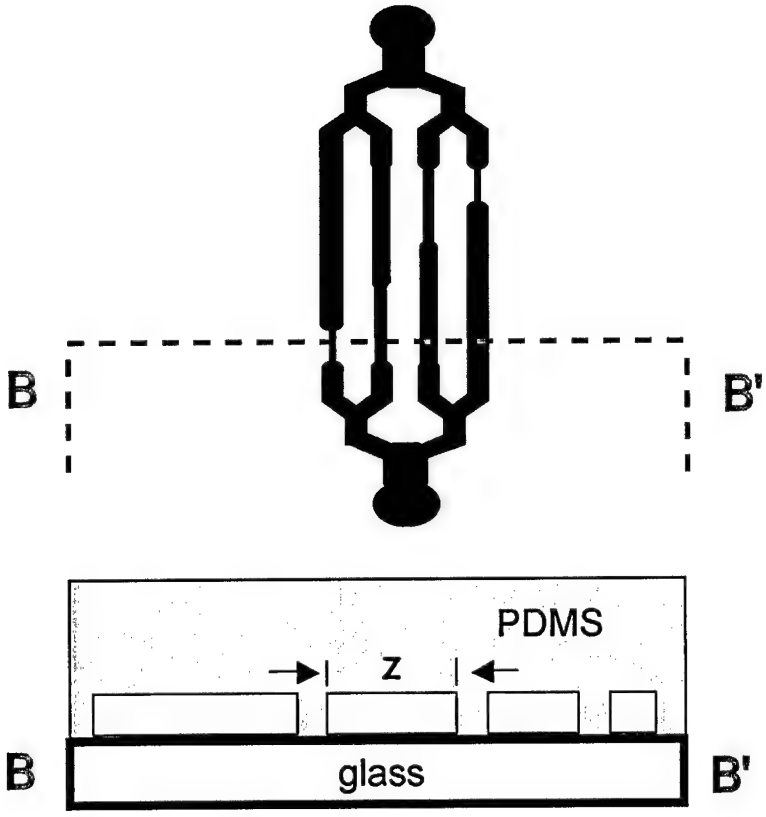

H =25 μm
z1, z2, z3, z4 = 1000, 750, 500, 250 μm

Figure 5C

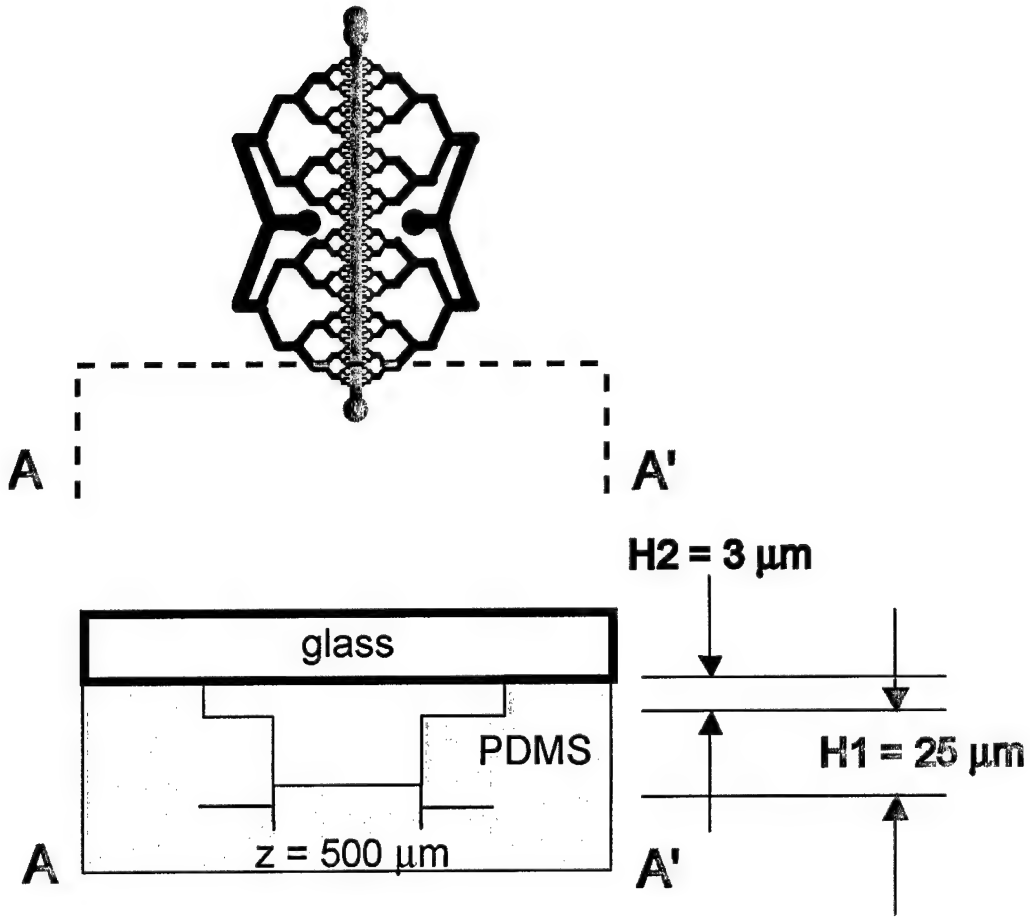

Figure 6

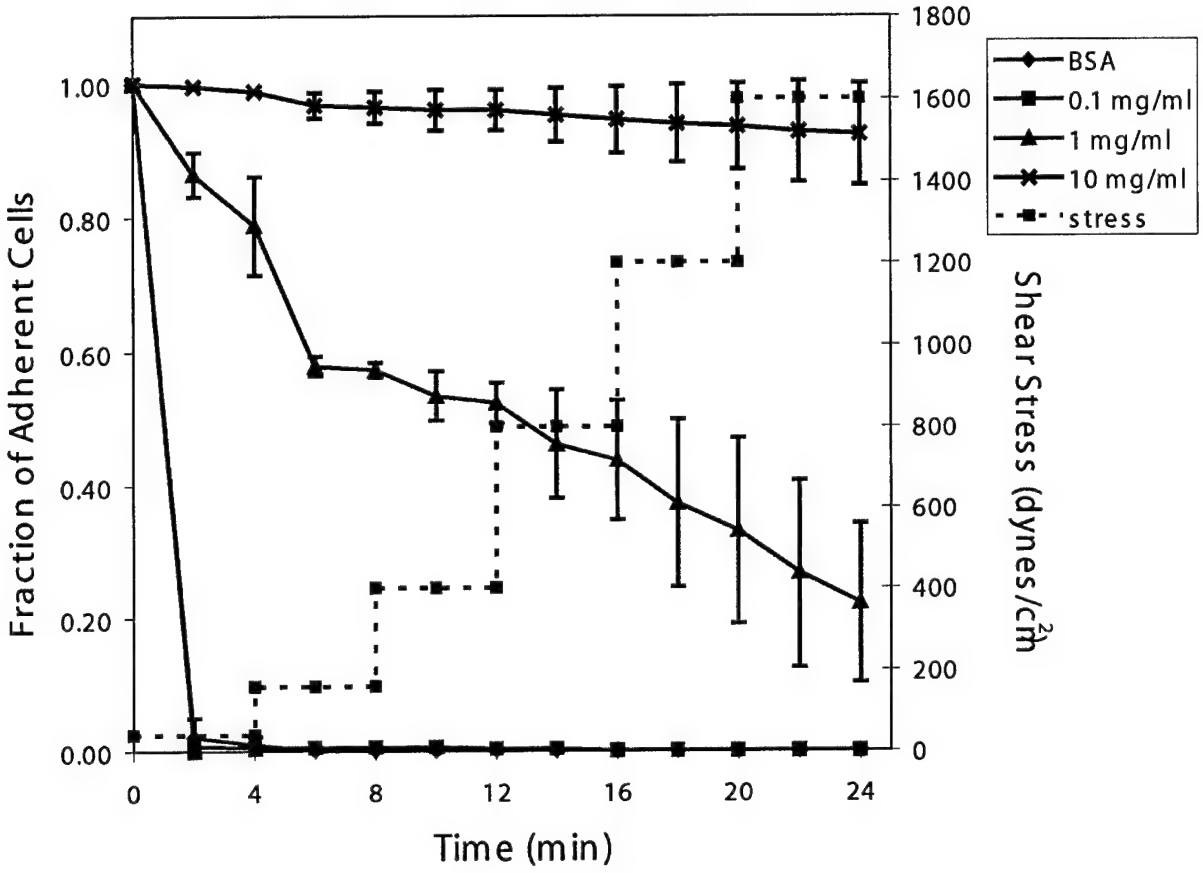
Fraction of Adherent Cells
1.00
0.80
0.60
0.40
0.20
0.00
0
4
8
12
16
20
24
Time (min)
1800
1600
1400
1200
1000
800
600
400
200
0
Shear Stress (dynes/cm2)
BSA
0.1 mg/ml
1 mg/ml
10 mg/ml
stress

Figure 7

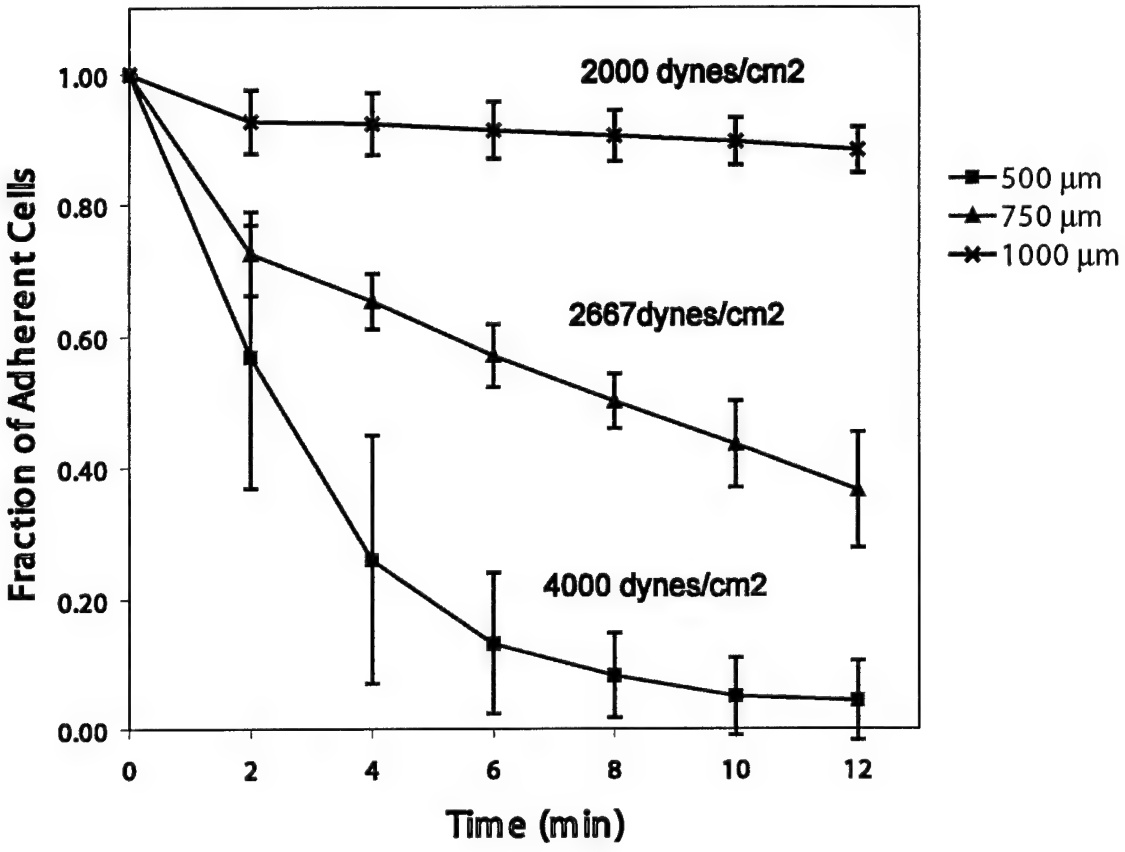
2000 dynes/cm2
2667dynes/cm2
4000 dynes/cm2
Fraction of Adherent Cells
1.00
0.80
0.60
0.40
0.20
0.00
0
2
4
6
8
10
12
Time (min)
500 µm
750 µm
1000 µm

Figures 8A and 8B

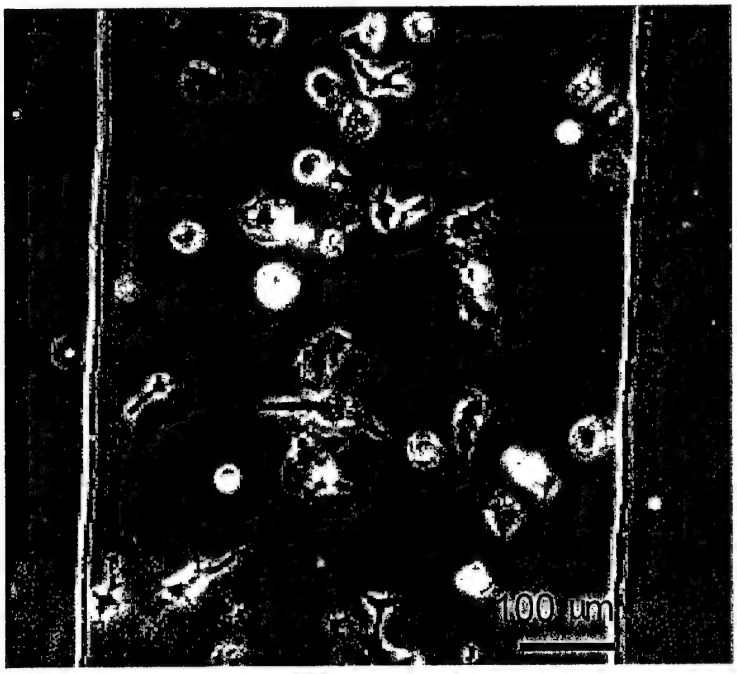

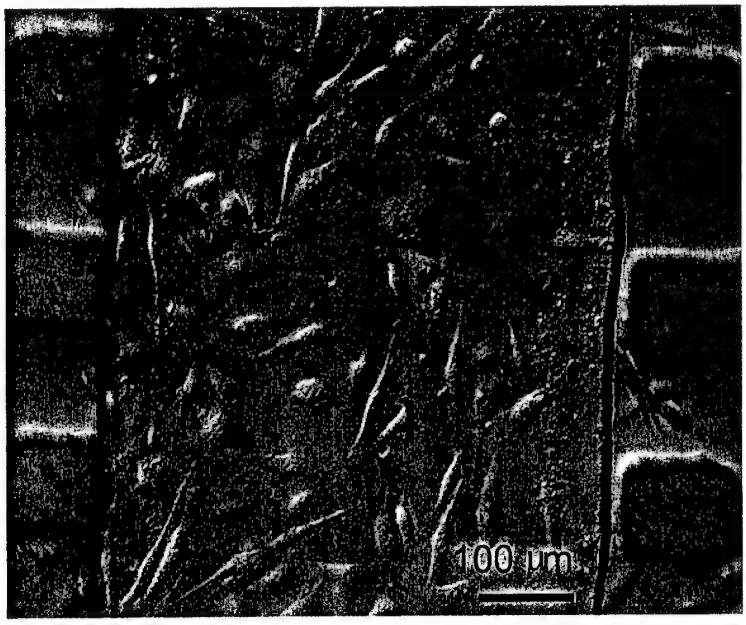

Figure 9

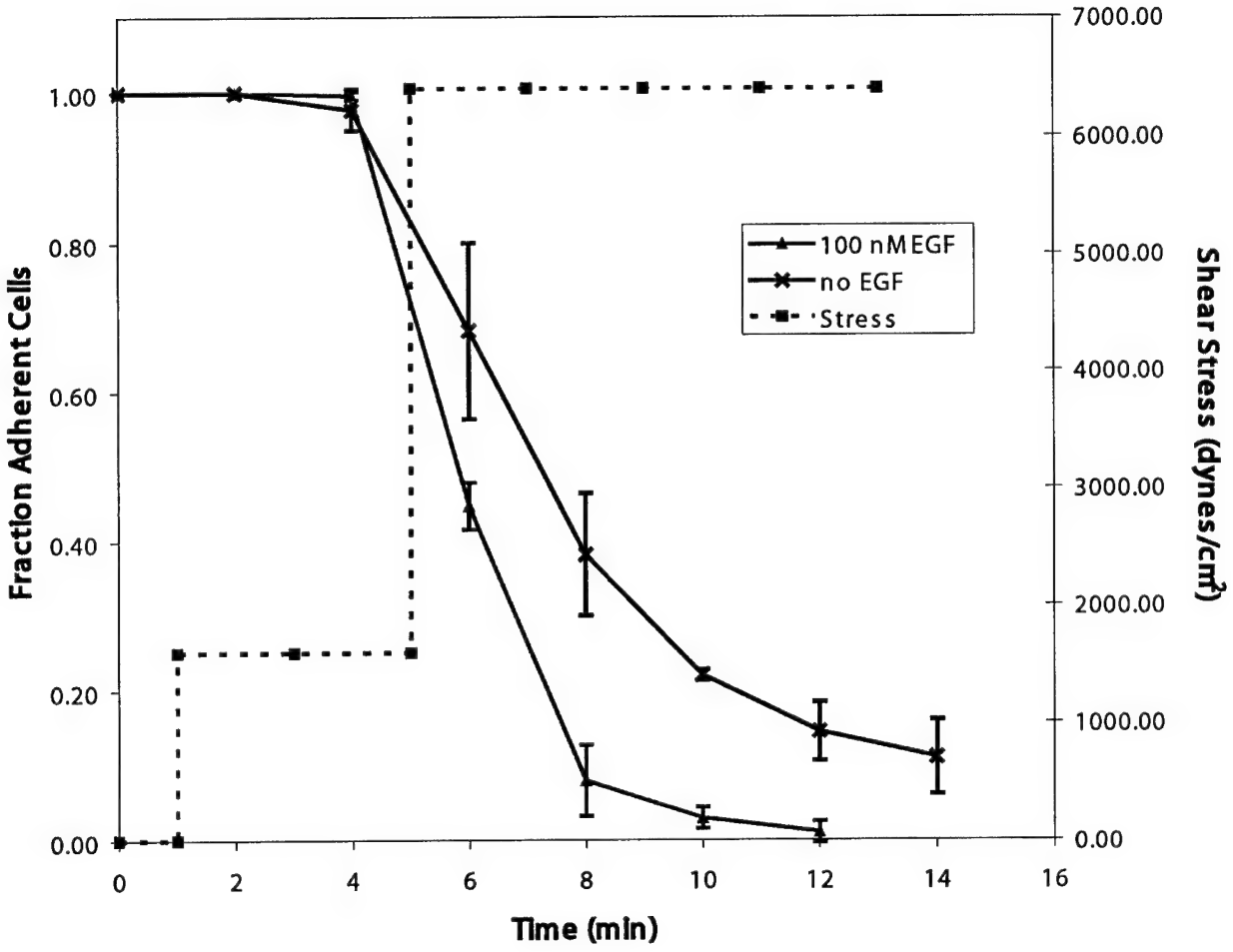
Fraction Adherent Cells
1.00
0.80
0.60
0.40
0.20
0.00
0
2
4
6
8
10
12
14
16
Time (min)
7000.00
6000.00
5000.00
4000.00
3000.00
2000.00
1000.00
0.00
Shear Stress (dynes/cm²)
100 nM EGF
no EGF
Stress

[CANCER RESEARCH 63, ●●●–●●●, August 1, 2003]

Calpain-2 as a Target for Limiting Prostate Cancer Invasion[1]

Asmaa Mamoune, Jian-Hua Luo, Douglas A. Lauffenburger, and Alan Wells[2]

Department of Pathology, University of Pittsburgh, Pittsburgh, Pennsylvania 15261 [A. M., J-H. L., A. W.]; Pittsburgh VAMC, Pittsburgh, Pennsylvania 15261 [A. W.]; and Biological Engineering Division, Department of Biology and Center for Cancer Research, Massachusetts Institute of Technology, Cambridge, Massachusetts 02139 [D. A. L.]

ABSTRACT

Mortality and morbidity of prostate cancer result from extracapsular invasion and metastasis. This tumor progression depends on active cell motility. Previous studies have shown that calpain-regulated rear detachment enabling forward locomotion is required for cell migration initiated by growth factor and adhesion receptors. Therefore, we asked whether calpain would be a target for limiting tumor progression, using as our model the PA DU-145 human prostate carcinoma cell line and a highly invasive subline, wild-type DU-145, derived from it. *In vitro*, the calpain-specific inhibitor CI-I (ALLN) and the preferential-but-less-specific inhibitor leupeptin decreased transmigration of both cell lines across a Matrigel barrier. These calpain inhibitors limited epidermal growth factor-induced motility but did not alter the growth rate of the tumor cells, as expected. Antisense down-regulation of the growth factor-activated calpain-2 (m-calpain) isoform also reduced transmigration and cell motility. These *in vitro* findings were then buttressed by *in vivo* studies, in which i.p. DU-145 tumor xenografts were treated with leupeptin. Tumor invasion into the diaphragm was reduced by leupeptin treatment for both the PA and wild-type DU-145 cells (from 1.7 to 0.78 for the parental line and 2.3 to 1.2 for the invasive derivative, respectively). Tumor cells of both types engineered to express calpain-2 antisense constructs also demonstrated a similar 50% reduced invasiveness *in vivo*. Finally, we found by gene expression survey of 53 human prostate tumors and 23 normal prostates that calpain was not up-regulated in relationship to invasiveness or metastatic activity, consistent with expectation from the biological role of this effector. Taken together, these results strongly suggest that epigenetic activation of calpain plays an important role in the invasion of human prostate cancer and that it can be targeted to reduce tumor progression.

INTRODUCTION

Prostate cancer is among the most frequent tumors in men (1), with the vast majority of morbidity and mortality resulting from tumor spread beyond the prostate (2, 3). Thus, work has focused on molecular changes that invasive and metastic tumors acquire to enable them to breach the barrier matrices and extend beyond the prostate capsule. Whereas there are a number of cell properties and their controlling signaling pathways, we have focused on cell migration as a critical rate-limiting step in tumor invasion (4–7). Extravasating and metastatic cells have been observed as displaying active motility during these actions (8–10). Therefore, inhibition of tumor cell motility should provide a novel therapeutic approach.

Cell motility is a highly orchestrated process that requires cell protrusion of leading lamellipodia with subsequent new adhesions, contraction through the cell body, and release from the substratum at the trailing edge (11). Each of these biophysical processes is controlled coordinately by biochemical signaling cascades (12). Such cascades can be initiated by adhesion receptors, notably integrins (13), or by growth factor receptors, although the specific elements in signaling chains may vary dependent on the initiating signal (12). The rear detachment step appears to be regulated by convergent signaling from growth factors and integrin (14, 15). Calpains are required for deadhesion of the tail during both haptokinesis (16) and chemokinesis (17, 18), at least on moderately to highly adhesive surfaces (19). However, it appears that integrins activate the calpain-1 (μ-calpain) isoform, whereas growth factor receptors trigger calpain-2 (m-calpain). As these two ubiquitously coexpressed proteins are highly homologous and appear to cleave the same targets, this convergence is likely because of differential regulation of the calpain isoforms (14, 20). Inhibition of calpain does block the motility of fibroblasts and myofibroblasts (16, 17), as well as keratinocytes (21). In the one study to date examining calpain-dependency of motility in carcinoma cells, inhibition of calpain in bladder carcinoma cells limited both motility and transmigration of a Matrigel barrier *in vitro* (22). The effects of inhibiting calpain were similar to when other motility-related signals are blocked, such as peritoneal lymphocyte γ-mediated cytoskeleton reorganization (22–24). Thus, there is promise that calpain may be a target for limited tumor invasiveness. However, this has yet to be determined in animal models.

Calpains are a family of >12 known mammalian intracellular limited proteases that share a similar catalytic structure (25). The two ubiquitous isoforms, calpain-1 and -2, are the best characterized and defined by their calcium requirements for *in vitro* activation. Whereas the biochemistry and structural biology of the ubiquitous calpains is highly advanced (25–28), the cell biology of these enzymes is lagging because of questions of mode of activation *in vivo* (14, 15). Calpains contribute not only to cell motility, as noted above, but also are likely involved in cell proliferation and apoptosis (15, 20, 29). Still less is known about the role of calpains in carcinogenesis and tumor progression. There is a report in a subset of 21 clear cell renal carcinomas of calpain-1, being up-regulated at the mRNA level in metastatic tumors compared with node-negative tumors (30). The gastric-specific calpain-9 is down-regulated in carcinomas from that tissue, although whether it is related to differentiation status or tumorigenesis is still open to question (31, 32). On the other hand, the decrease of muscle-specific calpain-3, and reciprocal increase in calpain-2 and ubiquitin-dependent proteolysis in muscles during cancer cachexia is almost assuredly a secondary organismal effect unrelated to tumor growth and progression (33). However, because calpain is regulated in an epigenetic manner and detection of changes in calpains are not expected, either calpain activity has to be determined directly or challenged in experimental systems to substantiated potential roles in tumor biology.

To investigate the role of calpain in prostate cancer invasion, we used the androgen-independent cell line DU 145 (PA; Ref. 34) and its derivative, WT,[3] which overexpresses the full length of EGFR and which has been shown to be more invasive (35, 36). Because the signature of activated calpain within cells is not known, we could not survey *de novo* tumors for activation status. Rather, we used an interventional strategy to establish proof of concept that calpains contribute to tumor invasion. Both ubiquitous calpains were inhibited

Received 10/23/02; accepted 5/23/03.

The costs of publication of this article were defrayed in part by the payment of page charges. This article must therefore be hereby marked *advertisement* in accordance with 18 U.S.C. Section 1734 solely to indicate this fact.

[1] Supported by grants from the VA Merit Award program, the United States Army CMRP in Prostate Cancer, and National Cancer Institute.

[2] To whom requests for reprints should be addressed, at Department of Pathology, 713 Scaife, University of Pittsburgh, Pittsburgh, PA 15261. Phone: (412) 647-7813; Fax: (412) 647-8567; E-mail: wellsa@msx.upmc.edu.

[3] The abbreviations used are: WT, wild-type; EGFR, epidermal growth factor receptor; EGF, epidermal growth factor; CI, calpain inhibitor; AS, antisense; MAP, microtubule-associated protein; V, vector; ECM, extracellular matrix.

pharmacologically by the calpain-specific inhibitor CI-I (ALLN) or the calpain-preferential but broad-spectrum cysteine-serine protease inhibitor, leupeptin. This latter agent was chosen because it has been used in mice and even, on the basis of compassionate release, in humans with little toxicity evident (37, 38). To confirm calpain targeting and identify the key isoform, AS down-regulation of calpain-2 was performed in these cells. Our findings indicate that calpain may represent a key molecular switch that regulates a rate-limiting step in tumor invasion.

MATERIALS AND METHODS

Cell Lines and Reagents. Human DU 145 prostate carcinoma cell line and its derivative WT DU145 (35, 36) were maintained in DMEM supplemented with 10% heat-inactivated fetal bovine serum supplemented with L-glutamine (2 mM), nonessential amino acids (0.1 mM), sodium pyruvate (1 mM), and antibiotics; 350 mg/ml of G418 was added to the medium for the WT cells. Medium was purchased from Life Technologies, Inc. (Gaithersburg, MD). The parental DU145 cells are referred to as PA DU145, whereas those cells overexpressing full length, WT EGFR are referred to as WT DU145. Human recombinant EGF was purchased from BD Biosciences, CI-I (ALLN) from Biomol (Plymouth Meeting, PA), and leupeptin and all of the other reagents were purchased from Sigma (St. Louis, MO).

Plasmids and DNA Constructs. To generate a minigene complementary to human calpain-2, we chose a sequence that spanned the translation initiating ATG, as AS to this sequence was productive (17). Human cDNA coding for 80 pb (C2AS) minigene was generated by RT-PCR using the following primers: 5′ oligo sequence 5′ACCGCAGCATGGCGGGCA; and 3′ reverse oligo sequence 5′TGGCCCTCTCGTGGGAGC. The cDNA was cloned into pBluescript II KS vector, digested with *Xho*I and *Bam*HI, and inserted into the *Xho*I and *Bam*HI sites of the mammalian pCEP4 expression vector. cDNA was sequenced to verify correct orientation and sequence. Expression was obtained by electroporation into DU145 cells. Stable transfectant cells were selected by supplementing the medium with 100 μg/ml hygromycin. These cells are referred to as C2AS WT or PA DU145, whereas the vector only controls are named V WT or PA DU145.

AS Oligonucleotides. Phosphorothioate AS oligodeoxynucleotides were synthesized by DNA synthesis facility (University of Pittsburgh). The sequences of calpain-2 AS have been described previously, 5′CGCGATGCCCGCCCGCCATGCT (39). A scrambled (SCR: 5′TCGTACCGCCCGCCCGTAGCGC) phosphothiorated oligonucleotide was used as a control. These sequences and their complementary sequences presented no similarity with other target mRNA, as best we could determine using the BLASTN program.

Quiescent cells were transfected using the superfectin reagent according to the manufactured protocol. Briefly, cells plated in 12-well plates were incubated with 20 μM of oligonucleotide with 7.5 μl of superfect in a final volume 500 μl for 3 h, then washed twice with PBS and incubated with or without 1 nM EGF for 24 h. For invasion assay, cells were counted and transferred into the transwell chambers. Otherwise, cells were kept in the same plate and used for MAP2 assay or wounded (0 h) for the migration assay.

Migration Assay. An *in vitro* "wound healing" assay was used to assess cell motility in two dimensions (40). Cells (10^5) were plated on a six-well plate and grown to confluence in their regular medium. To minimize the autocrine signaling, confluent cells were kept in 1% dialyzed FBS, then wounded using a rubber policeman (0 h). Cells were washed twice with PBS and treated with or without specific effectors for 24 h. Photographs were taken at 0 and 24 h, and the distance traveled was determined by subtracting the values obtained at 0 from 24 h. Mitomycin C (0.5 μg/ml) was used to limit proliferation (41).

Calpain Activity Assays. Calpain activity was detected in living cells or in the whole cell lysates using BOC or MAP2 assays, respectively, as described previously (17). Briefly, for BOC, cells were plated on glass coverslips at between 50 and 70% confluence in their regular media. Quiescent cells were treated with or without 1 nM EGF, CI-I, or leupeptin for 24 h. BOC-LM-CMAC (0.5 μM; Molecular Probes, Eugene, OR) is added to the cells for 20 min followed by 1 nM EGF for 10 min. The activity of calpain was detected by the increase of fluorescence noted on the cleavage of the substrate BOC using an Olympus fluorescent microscope (model BX40 with an Olympus M-NUA filter), and representative images were captured using a spot CDD camera. The exposure and time settings were fixed within each experimental series.

To determine calpain activity in cell lysates, MAP2 (Cytoskeleton, Denver, CO) was labeled with DTAF by incubation of MAP2 and DTAF in (pH 8.5) PIPES buffer for 30 min at 4°C. Labeled MAP2 was then isolated by size exclusion column chromatography and dialyzed against (pH 7.5) HEPES buffer overnight. Cells were grown to confluence in six-well plates, quiesced for 24 h, and treated or not with 1 nM EGF. Cells were washed twice with ice-cold PBS and lysed with cell lysis buffer [20 nM HEPES (pH 7.4), 10% glycerol, 0.1% Triton X-100, 500 mM sodium chloride, and 1 mM sodium vanadate]. After removing the cell debris by centrifugation, 0.9 μg of DTAF-labeled MAP2 was added to the samples with 20 μM free Ca^{2+} concentration. Fluorescence was immediately measured by an Aminco-Bowman Series II spectrofluorimeter (Spectronic Instruments Inc., Rochester, NY) at excitation and emission wavelength of 470 and 520 nm, respectively, for 3 min at room temperature

To detect the total potential calpain activity in a cell, we used casein zymography. Twenty μg of cell lysate were resolved under nonreducing conditions by PAGE in HEPES-imidazole buffer with 5 mM EDTA that separates calpain-1 and -2 isoforms. After washing, gels were incubated for 20 h in a calpain activation buffer (20 mM 4-morpholinepropanesulfonic acid 2 plus 5 mM BME) containing 5 mM $CaCl_2$ or in 4-morpholinepropanesulfonic acid buffer without $CaCl_2$ and with EDTA as a control. The gels were stained for protein content with transparent bands identified by comparison to calpain standards. The density of the bands was measured using NIH image.

Immunoblotting. Protein expression was determined as described previously (17). Briefly, cells were washed in PBS and lysed in SDS lysis buffer before analysis by reducing SDS-PAGE. Primary antibodies included anticalpain-2 (clone N-19 and C-19; Santa Cruz Biologics, Santa Cruz, CA), anticalpain-1 (Biomol), and antiactin (Sigma). Bands were visualized using alkaline-phosphatase-coupled secondary antibody (Promega, Madison, WI).

Cell Proliferation Assay. Mitogenic stimulus was determined by direct cell counting. Cells were plated in 24-well plates and cultured for 24 or 48 h in their regular medium, with or without leupeptin or CI-I. The number of cells was determined using a Coulter Counter model Z2 (Miami, FL).

Invasion Assays. Invasive potential was determined *in vitro* by transmigration of an ECM (5). Matrigel invasion chamber plates were obtained from Becton Dickinson/Biocoat (Bedford, MA). The upper surface of the matrix was challenged with 20,000 cells, a number derived from empirical experimentation (22, 23, 35). Cells were kept in serum-free medium containing 1% BSA for the first 24 h and then replaced with only serum-free medium for the remaining 24 h; the lower chamber contained medium containing 10% serum for the entire assay. Enumeration of the cells that invaded through the matrix over a 48-h period was accomplished by visually counting cells on the bottom of the filter, as per routine procedures, after any uninvaded cells were removed from the top of the filter with a cotton swab. In all of the cases, individual experiments were performed in duplicate chambers.

True invasiveness of the cells was determined *in vivo* using the diaphragm invasion model (5, 24, 36). For the first experimental series, 14 male 6-week-old Balb/*c nu/nu* athymic mice (day 0) were inoculated i.p. with 2×10^6 PA or WT DU145 cells and randomly separated into two groups at day 10. After 10 days, the mice received daily i.p. injections of 12 mg/kg of leupeptin or diluent only for 30 days. In the second experimental series, mice were inoculated with either PA or WT DU145 expressing C2AS minigene or V alone to assess AS down-regulation of calpain-2 on tumor invasion after 60 days. In all of the cases, invasion was determined as follows. Mice were sacrificed, and the diaphragm and any tumors were removed, fixed in 10% paraformaldehyde, and stained with H&E. Invasiveness was scored semiquantitatively on a four point scale measuring the greatest extent of invasion into the diaphragm muscle, with 0 being no invasion and 4 being complete transmigration of the diaphrugm. Mice without evident diaphragmatic tumors were not included in the invasion scoring. Each experiment was repeated and the data collated for the two experiments. The number of mice challenged was determined *a priori* for a 95% confidence level of determining a difference ($P < 0.05$) using the assumptions of 80% diaphragmatic tumors with a 30% difference in invasiveness between the comparison groups; this yielded a minimum mouse number of 12 mice per test set. These assumptions were based on prior experimentation of altered EGFR or peritoneal lymphocyte signaling (24, 36). All of the animal

experiments were certified by the University of Pittsburgh and Pittsburgh VA Medical Center Institutional Animal Care and Use Committees.

Microarray Gene Expression Analysis. We queried the gene expression profile of 53 prostate cancers and 23 normal donors using the Affymetrix (Santa Clara, CA) system. These human tumor queries were determined as exemption 4 under pre-existing data and excess pathological specimens by the University of Pittsburgh Institutional Review Board; specimens were provided by an "honest broker," and the investigators were blinded as to patient identity. Designation of invasive (aggressive; $n = 29$) and localized (organ-confined; $n = 24$) was per pathology report for clinical use. In addition, 23 normal human prostates from organ donors were run in parallel.

Samples of prostate tissues obtained from prostatectomy were dissected and trimmed to obtain pure tumor (completely free of normal prostate acinar cells) or normal prostate tissues. Sandwich-frozen sections were performed by board-certified GU pathologists to examine the purity of the tumors. These tissues were then homogenized. Total RNA was extracted and purified with Qiagen RNeasy kit (Qiagen, San Diego, CA). Five μg of total RNA were used in the first strand cDNA synthesis with T7-d$(T)_{24}$ primer [GGCCAGTGAATTGTA-ATACGACTCACTATAGGGAGGCGG-(d$T)_{24}$] by Superscript II (Life Technologies, Inc., Rockville, MD). The second-strand cDNA synthesis was performed at 16°C by adding *Escherichia coli* DNA ligase, *E. coli* DNA polymerase I, and RnaseH in the reaction. This was followed by the addition of T4 DNA polymerase to blunt the ends of newly synthesized cDNA. The cDNA was purified through phenol-chloroform and ethanol precipitation. The purified cDNA was then incubated at 37°C for 4 h in an *in vitro* transcription reaction to produce cRNA labeled with biotin using MEGAscript system (Ambion, Inc., Austin, TX).

Hybridization was as follows. Fifteen to 20 μg of cRNA were fragmented by incubating in a buffer containing 200 mM Tris-acetate (pH 8.1), 500 mM KOAc, and 150 mM MgOAc at 95°C for 35 min. The fragmented cRNA were then hybridized with a pre-equilibrated Affymetrix chip at 45°C for 14–16 h. After the hybridization mixtures were removed, the chips were then washed in a fluidic station with low-stringency buffer (6× saline-sodium phosphate-EDTA, 0.01% Tween 20, and 0.005% antifoam) for 10 cycles (2 mixes/cycle) and stringent buffer (100 mM 4-morpholinepropanesulfonic acid, 0.1 M NaCl and 0.01% Tween 20) for 4 cycles (15 mixes/cycle), and stained with streptoavidin phycoerythrin. This was followed by incubation with biotinylated mouse antiavidin antibody, and restained with strepto-avidin phycoerythrin. The chips were scanned in a HP ChipScanner (Affymetrix Inc.) to detect hybridization signals.

Data were analyzed by importing the hybridization data from text files into an Microsoft excel spreadsheet. GeneSpring 4.2 along with Michael Eisen's cluster and tree view software were the primary analysis tools. Principle component analysis and logistic regression were performed using S-Plus (Statistical Sciences, Inc.) statistical software.

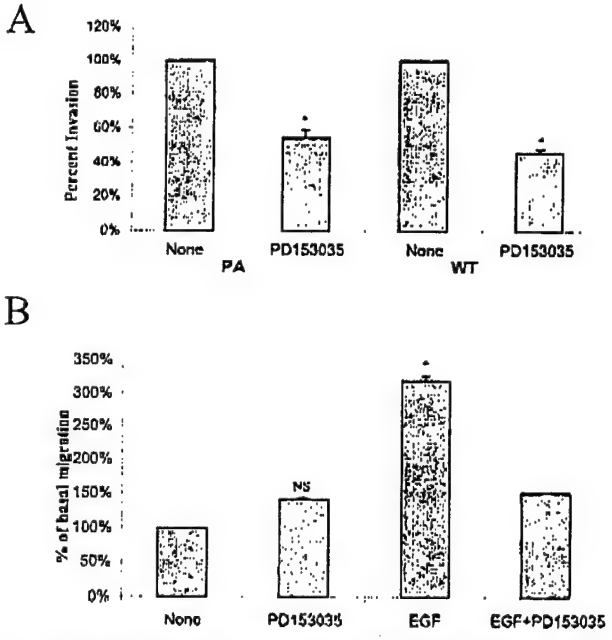

Fig. 1. DU145 invasion and migration are dependent on EGFR signaling. *A*, PA or WT DU145 cells (20,000) were plated in the upper chamber of the transwell plate in medium containing 1% BSA and 500 ng/ml EGFR inhibitor (PD153035). After 24 h, the medium in the upper chamber was replaced with serum-free medium containing PD153035 for another 24 h. The bottom chamber contained complete medium with 10% FCS and PD153035. Cells in the upper compartment were removed by wiping with a cotton swab, and invasive cells were stained according to the manufacture's protocol. *B*, PA DU145 cells were plated in six-well plates and quiesced for 24 h before an *in vitro* wound-healing assay. Cell movement into the denuded space was assessed in the presence of EGF (1 nM) and/or PD153035 (500 ng/ml) or diluent. All of the experiments were performed in triplicate and repeated at least twice. Effects are normalized to diluent alone for the respective cell line; in *A* absolute invasiveness was 2.00 ± 0.24 in WT over PA DU145 cells. $**P < 0.05$ as compared with no treatment, NS, not significant; *bars*, ±SD.

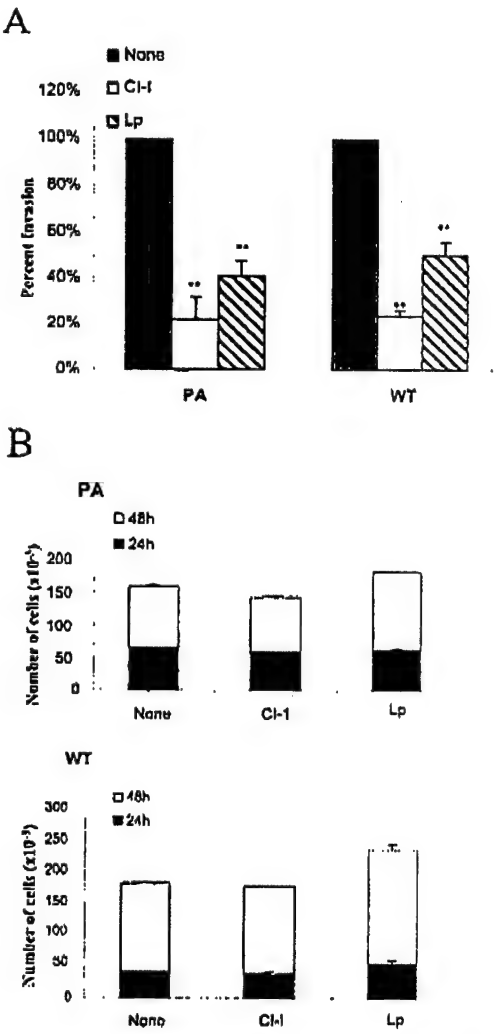

Fig. 2. Calpain inhibition reduces invasiveness of PA and WT DU145 cells *in vitro*. *A*, cells (20,000) were plated in the upper chamber of the transwell plate in medium containing 1% BSA and 2 μg/ml CI-1 or 100 μM of leupeptin (*Lp*). After 24 h, the medium in the upper chamber was replaced with serum-free medium containing CI-1 or Lp for another 24 h. The bottom chamber contained complete medium with 10% FCS and CI-1 or Lp. Cells in the upper compartment were removed by wiping with a cotton swab, and invasive cells were stained according to the manufacture's protocol. *B*, cells (20,000 PA or 10,000 WT) were plated in 24-well plates and cultured for 24 or 48 h in CI-1 or leupeptin (*Lp*). Cell numbers were enumerated directly. All of the experiments were performed in triplicate and repeated at least twice. $**P < 0.01$; *bars*, ±SD.

RESULTS

Invasiveness of DU-145 Prostate Cell Lines Is EGFR-dependent. EGFR overexpression correlates with tumor progression and invasion (5, 7). We tested the hypothesis that motility induced by

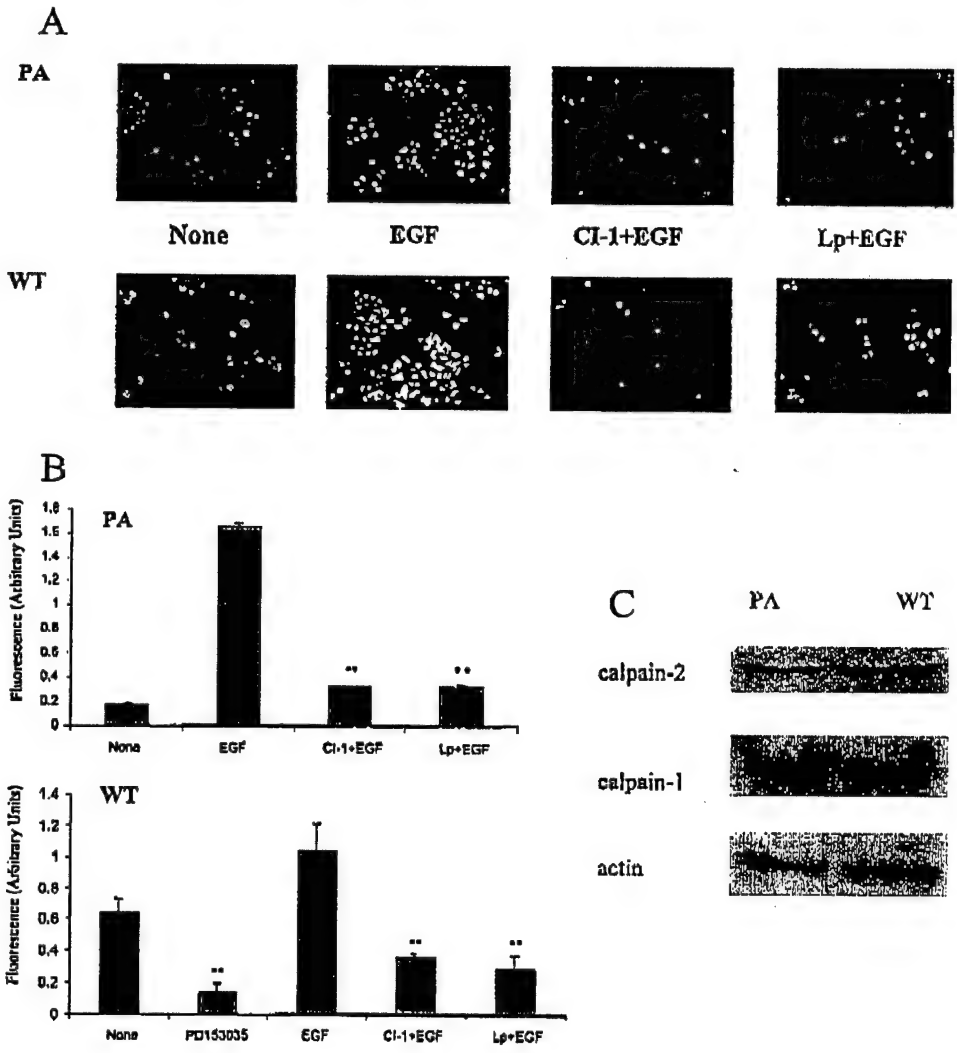

Fig. 3. Leupeptin and CI-1 block EGF-induced calpain activation. *A*, quiescent WT and PA DU145 cells were treated with CI-1 (ALLN; 2 μg/ml) or leupeptin (*Lp*; 100 μM) for 24 h before loading with BOC-Leu-Met-CMAC for 20 min. Cells were then stimulated with EGF (1 nM) for 10 min before visualizing with a preset CCD camera. The shown exposures are set so only cells with activated calpain are seen; in all of the frames similar numbers of cells were present as determined by phase contrast performed in parallel. *B*, cells were quiesced for 24 h before exposure to EGF (1 nM). Cells were treated with CI-I, leupeptin (as in *A*), or PD153035 (500 nM). Cells were lysed and cleared cytosolic lysates evaluated for their ability to cleave DTAF-labeled MAP2 as described. *C*, cells were grown in complete medium in six-well plates, washed, lysed, and proteins separated by SDS-PAGE. Equal protein loads were immunoblotted for calpain-2, calpain-1, or actin as a loading control. All of the experiments were repeated at least twice with the calpain assays performed in duplicate. $^{**}P < 0.01$, as compared with diluent alone for PD153035 and compared with EGF treatment for CI-I and leupeptin.

autocrine EGFR signaling is a rate-limiting step in the invasion using our model of variously invasive syngeneic DU145 prostate cancer cell lines. Exposure of the moderately invasive PA DU145 or the highly invasive WT DU145 cells to the EGFR kinase inhibitor PD153035 decreased significantly the invasiveness through Matrigel even in the absence of exogenously added EGFR ligand (Fig 1*A*). The data are normalized to the respective mock-treated controls; WT DU145 cells are 1.7 (35) to 2.0 (data herein; $P < 0.05$) times more invasive than PA DU145 cells. EGFR-signaled cell motility was examined under conditions that minimize autocrine EGFR signaling (Fig. 1*B*). As shown in PA DU145 cells, EGF increased motility, which was abrogated by PD153035. These data support the previous literature (22, 35, 36) and demonstrate that the invasiveness of these cells is driven by EGFR signaling.

CIs Reduce DU 145 Cell Invasiveness *in Vitro*. The initial question we asked was whether calpain signaling was required for transmigration of an ECM. Transmigration of Matrigel by the moderately invasive PA DU145 and highly invasive WT DU145 lines was determined in the presence of CI-1 (ALLN; 2 μg/ml) or leupeptin (100 μM; Fig. 2*A*). The number of cells that reached the lower chamber within 48 h was significantly decreased by both inhibitors in both cell lines; the absolute invasiveness of WT DU-145 cells was 2.0-fold that of PA DU-145 cells. This agent-related decrement in cells transmigrated was not secondary to decreased proliferation (15, 20, 29, 39), as the concentrations of CI-1 and leupeptin used in this assay did not block cell proliferation (Fig. 2*B*).

Calpain activation was inhibited by both CI-1 and leupeptin (Fig. 3). First, we ascertained calpain activity *in vivo* by visualizing the bright blue fluorescence after the proteolysis of BOC-LM-CMAC, a calpain-selective substrate (42). Induced calpain activity was inhibited by both CI-1 and leupeptin in both PA and WT cells lines (Fig. 3*A*). In addition, we quantitated calpain activation using cleavage of the prefluorescence substrate DTAF from MAP2; again, both inhibitors limited or eliminated EGF-induced activation of calpain (Fig. 3*B*). WT DU145 demonstrated a somewhat higher basal activity as expected because of increased autocrine EGFR signaling (35), as it was inhibited by the pharmacologic agent PD153035 (Fig. 3*B*). Induced calpain activity was inhibited by both CI-1 and leupeptin to a level similar to that seen in the presence of PD153035 (Fig. 3*B*). The higher basal activity observed in WT compared with PA cells is not attributable to a higher amount of calpain-1 or -2 expression (Fig. 2*C*). Thus, we had evidence for calpain inhibition limiting tumor cell invasion.

Down-Regulation of Calpain-2 Limits PA DU145 Invasion. Molecular targeting of calpain was required, as leupeptin, in particular, and possibly even as CI-1 inhibit proteases in addition to calpain. We used AS approaches to calpain-2 to abrogate signaling through this molecule (17). Oligonucleotides against calpain-2 in PA DU145

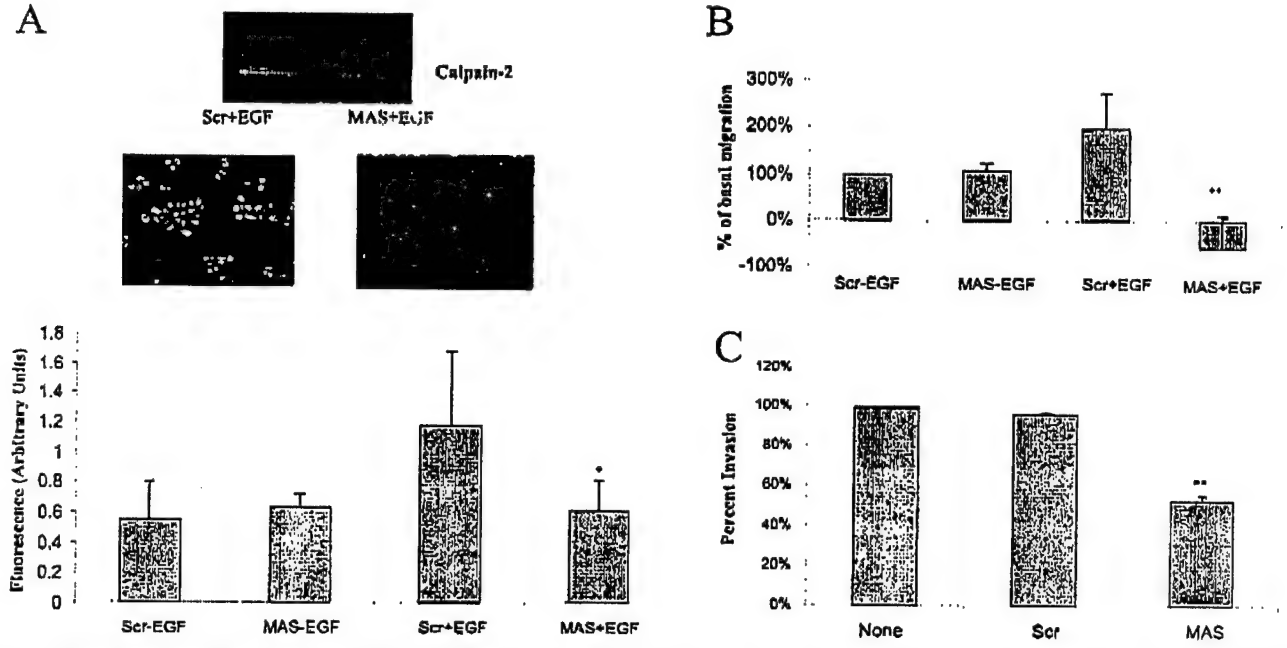

Fig. 4. AS oligonucleotides to calpain-2 decrease PA DU145 cell invasiveness and migration. Phosphothiorated oligonucleotides (20 μM) specific for calpain-2 (*MAS*; Ref. 17) were added to cells; a scrambled oligonucleotide (*Scr*) of similar composition served as a control. *A*, calpain activation was assessed by zymography (*top panel*), BOC-Leu-Met-CMAC (*middle panel*), or MAP2 (*bottom panel*) as described. *B*, the effect of MAS or Scr oligonucleotides on PA DU145 cell migration across a two-dimensional surface were calculated as a percentage of the values obtained with the Scr oligonucleotide alone. *C*, the invasion through Matrigel was evaluated as previously described and the number of cells that transmigrated through the Matrigel were normalized to no treated cells. All of the experiments were repeated at least twice, with the assays performed in duplicate. $^{**}P < 0.01$; NS, not significant; *bars*, ±SD.

cells limited EGF-induced calpain activation cell migration and transmigration of the Matrigel barrier (Fig. 4). A control scrambled oligonucleotide did not effect these parameters.

We generated a stable PA DU145 derivative in which an 80-bp minigene around the calpain-2 translation initiation site was expressed in the AS direction from the cytomegalovirus promoter. In these cells, calpain-2 levels were reduced by >30% as quantified using an NIH program (Fig. 5); such partial down-regulation was expected because calpain-2 is required for cell viability and growth (15, 20, 29, 39); importantly, a similar level of calpain-2 down-regulation eliminates EGF-induced calpain activity and motility in fibroblasts (17). These cells were significantly less invasive than a PA DU145 derivative expressing the vector alone as a control. This decrement in invasiveness was not because of decreased cell numbers, whether reduced proliferation or survival, because the two derivative polyclonal lines grew at the same rate. In sum, these data strongly suggest that calpain-2 activation is required for increased tumor cell motility and subsequent invasiveness *in vitro*.

Leupeptin and Down-Regulation of Calpain-2 Decreases DU145 Invasiveness *in Vivo*. Our data *in vitro* show that calpain activity is required for cell transmigration throughout a "defined" layer of ECM. To investigate the role of calpain in an *in vivo* environment where complex and various interactions occur, we used the murine tumor xenograft model of diaphragm invasion (24, 36). This assay was used because it is more easily quantitated than invasiveness of orthotopic tumor growth for both technical and biological reasons; however, the semiquantitative scores of diaphragm invasion correlate well with the qualitative assessment of invasiveness of orthotopic tumors (24, 36). The pharmacological agent chosen was leupeptin because this has been used in both mice and humans with minimal toxicity (37, 38). Either PA or WT DU145 cells were inoculated i.p. into athymic mice and allowed to establish for 10 days before treatment with leupeptin or diluent alone. The WT DU145 tumors demonstrated increased invasion *in vivo* ($P < 0.05$ compared with PA DU145 tumors), similarly to the increment *in vitro* transmigration of Matrigel; this finding is consistent with our previous reports (24, 36). For both cell lines, leupeptin treatment significantly reduced the extent of invasion into and through the diaphragm (Table 1). T1
Invasion into other soft organs was not scored because of difficulty in quantitation but qualitatively reflected this difference. The reduction of invasiveness seen with leupeptin was not attributable to decreased tumor growth, because tumors in the diaphragm with the same size from treated or not treated mice showed different level of invasiveness (Fig. 6). This is expected, because leupeptin did not affect cell F6
proliferation (Fig. 2*B*).

Verifying that this invasiveness was because of calpain inhibition required a second approach because leupeptin inhibits other proteases, both intracellularly as well as extracellularly. We repeated the diaphragm invasion assay using the PA and WT DU145 cells expressing the calpain-2 AS minigene or vector alone (Table 2). Mice inoculated T2
with the calpain-2 AS showed 50% less invasiveness compared with the mice carrying the vector alone (Fig. 7). The PA DU145 cells F7
exhibited high significance in themselves, whereas the WT DU145 were marginally inhibited; this affect is likely because of the few mice challenged in this second series, which was curtailed because of the outcome of the P DU145 cells. Again the tumor take rates and size of the diaphragm tumors were indistinguishable between the sublines expressing C2AS or V constructs. This degree of inhibition of invasiveness by slightly more than half was in line with the extent of inhibition shown by leupeptin.

Calpain Levels Are Not Altered in Human Prostate Tumors. The above data strongly suggest an epigenetic role for calpain in enabling tumor cell motility and subsequent invasion. To address whether this is also altered gene expression levels of calpain-2 in prostate tumors, we analyzed 29 aggressive/invasive or metastatic tumors and 24 organ-confined tumors (Table 3). In addition, 23 T3
normal prostates were queried on the same chip set. We also examined the expression of calpain-1 and calpastatin, because these might alter

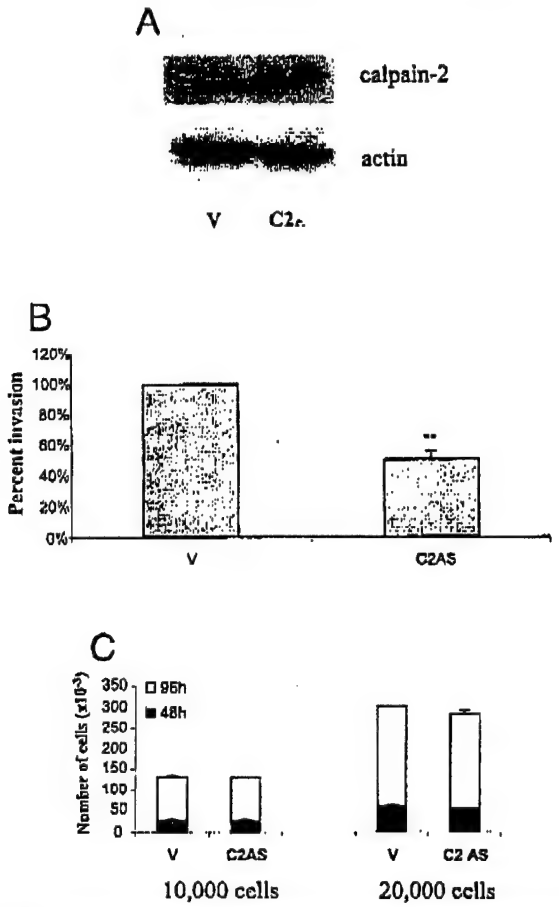

Fig. 5. AS minigene down-regulation of calpain-2 reduces PA DU145 invasiveness. PA DU145 cells were stably transfected with a minigene that expressed AS across the translation initiation site of calpain-2 or an empty vector. *A*, calpain-2 levels were ascertained by immunoblotting. Invasiveness through Matrigel (*B*) and cell proliferation (*C*) were evaluated as described. All of the experiments were repeated at least twice, with the invasiveness assay performed in duplicate and the cell counting in triplicate. $^{**}P < 0.01$; *bars*, ±SD.

the calpain activity balance. Analysis of the expression levels of all five of the calpain-related hybridization spots using the Welch *t* test indicated minimum variation of gene expression across all of the samples. Calpain-2 and calpain-1 expression were characterized as being at moderate levels, whereas expression of calpastatin was minimum. No significant expression change was identified when aggressive prostate cancer was compared with normal donor or organ-confined prostate cancers.

DISCUSSION

Tumor invasion is a complex process that involves cellular migration, interaction with the microenvironment, and survival at the ectopic site. We and others have shown that cell migration is a rate-limiting step in this process (5). Thus, key molecular switches required for functional migration may be successfully targeted to limit tumor spread. Previous studies have shown that the calpain proteases are required for rear deadhesion during productive motility whether initiated by adhesion-related signals or growth factors (14, 16–18). Synthesizing these finding for tumor invasiveness, an initial report demonstrated that blockade of calpain limited both the motility and invasiveness *in vitro* of bladder carcinoma cells (22). As local invasion generates a great part of the morbidity of prostate cancer, we asked whether blockade of calpain signaling would limit this spread. Herein, we report that pharmacological and molecular inhibitors of calpain-2 significantly reduce the motility and invasiveness of DU145 human prostate carcinoma cells both *in vitro* and *in vivo*. These data suggest that calpain may be rationally targeted to limit prostate cancer spread.

Our data strongly implicate calpain-2 control of cell motility as the operative target. However, this assignment is compromised by the lack of selectivity of the pharmacological agents for the calpain-2 isoform; this is especially true for the broad spectrum inhibitor leupeptin. Despite this uncertainty of inhibition, leupeptin was chosen, because it has been used in both animals and humans with minimal reported toxicity (37, 38). Still, a strong case for calpain-2 being the critical element is made by the fact that AS approaches to calpain-2 mimic the findings with leupeptin and CI-I. Whereas leupeptin inhibits both intracellular and extracellular proteases, and ECM remodeling might be hindered (43), the expression of the AS calpain-2 minigene should not alter the myriad of extracellular proteases. Thus, a confluence of data support targeting calpain-2.

A second point of contention may rest on which cell behavior is limited by calpain inhibition. In many settings calpain activity is required for cell proliferation or apoptosis in addition to motility (20). Our *in vitro* data suggest that in this setting our level of calpain inhibition does not affect cell proliferation (Fig. 2*B*; Fig. 5*C*). However, the *in vivo* experiments are not readily amenable to such analyses; although the fact that the tumor take rate (Tables 1 and 2) and size of the tumors were indistinguishable between the calpain-inhibited and control tumors is reassuring that overall cell number is not the main target of calpain inhibition.

It is possible that the increased motility and invasion may be indirectly related to calpain activation because the broad spectrum of calpain targets may also involve regulation of secreted proteases. We feel that this is an unlikely mechanism, because our earlier works failed to demonstrate differences in protease production between PA and WT DU145 (35). Furthermore, because motility over a two-dimensional surface is also affected, the need for extracellular proteases to modify a "barrier" matrix is limited, although others have suggested that matrix metalloprotease 9 is required for dispersion of cohesive keratinocytes even over a matrix surface (44). However, in our earlier survey of cellular proteases produced by DU145 sublines, matrix metalloprotease 9 was secreted at equivalent levels by the three syngeneic lines (35). Lastly, EGF only activates calpain-2 in the immediate subplasma membrane locale (45), and, thus, protease maturation is not likely globally affected by such localized signaling. However, until the identification of the specific target of calpain during induced motility (14), both indirect as well as direct molecular mechanisms must be considered. AQ:

Prostate cancer motility and invasion likely uses both ubiquitous calpain isoforms, calpain-2 and calpain-1, for cell movement. This is because prostate carcinoma cells present both integrins capable of promoting haptokinesis and EGFR-mediate autocrine signaling loops that induce chemokinesis (46). Calpain-1 (μ-calpain) has a calcium-dependency that can be attained in living fibroblasts and epithelial

Table 1 *Leupeptin decreases tumor invasiveness in mice*

Control mice inoculated with PA or WT cells were injected with diluent HBSS, and the experimental mice received 12 mg/kg of leupeptin. Mice were sacrified and diaphragm scored for diaphragm invasiveness from 0 to 4. Diaphragm tumors represent the total number of mice with tumors in the diaphragm.

	PA + HBSS	PA + leupeptin	WT + HBSS	WT + leupeptin
Diaphragm tumors	14/14	13/14	14/14	13/14
Diaphragm invasiveness	1.71	0.7[a]	2.35	1.25[b]

[a] $P < 0.01$.
[b] $P < 0.05$.

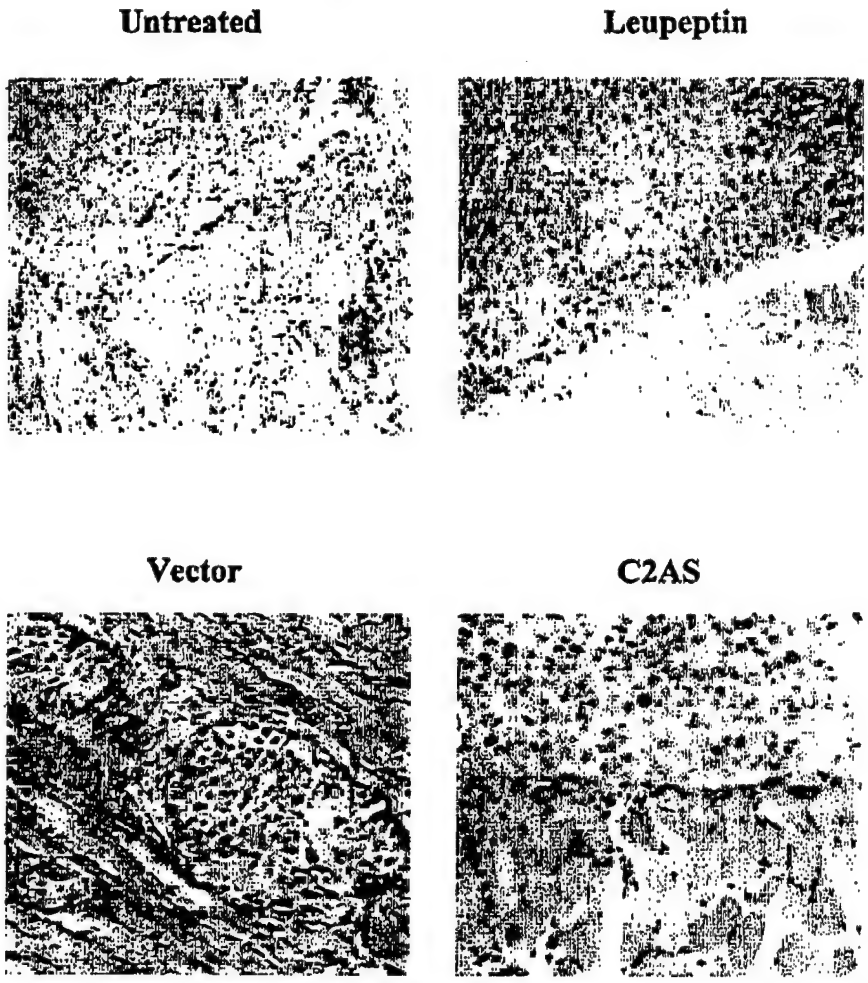

Fig. 6. Leupeptin reduces diaphragmatic invasion *in vivo*. Six-week-old male *BALB/c nu/nu* mice were injected i.p. with 2 million PA DU-145 cells. Ten days later, mice were separated into two groups, one was daily given i.m. injection of 12 mg/kg of leupeptin for 30 days, and the other control group was injected with a similar volume of HBSS. Diaphragms were isolated and evaluated by histopathology. Shown are representative invasion values of 2+ (diluent) and 0 (*Leupeptin*).

Fig. 7. AS down-regulation of calpain-2 reduces diaphragmatic invasion *in vivo*. Six-week-old male *BALB/c nu/nu* mice were injected i.p. with 2 million PA DU-145 cells expressing the minigene or vector alone. Sixty days later the diaphragms were isolated and evaluated by histopathology. Shown are representative invasion values of 3+ (*vector*) and 1 (*C2AS*).

cells (47). The autocrine EGFR-mediated signaling would activate calpain-2 preferentially via an ERK mitogen-activated protein kinase pathway at the inner face of the plasma membrane (17, 45). Thus, there appears to be a convergent signaling through the two ubiquitous calpain isoforms to regulate cell deadhesion (14). Whereas this might suggest that the best target for intervention is the end target, there are reasons to focus on calpains. First, the presumably common end target(s) might be individually sufficient, but none are actually required, making specific intervention ineffectual. Second, it is likely that the end target of calpain is a structural component and, thus, not readily "inhibitable," although the activation of the rho-GTPase may suggest sensitive points for intervention (48). Third, the ability to inhibit only one isoform may limit toxicity, because homeostatic mechanisms that require low level motility, such as colonic or skin epithelial replacement, would use one of the isoforms and not the other in the absence of injury repair needs (49). Unfortunately, the commonly available inhibitors such as leupeptin and CI-I do not distinguish between the isoforms, making molecular approaches the only viable option at present to determine whether inhibition of a single isoform can accomplish blockade of tumor invasiveness. Obviously, new, isoform-specific small molecule inhibitors would greatly advance our understanding of the physiology of calpain activation.

The question remains of whether these findings in model systems

Table 2 *Antisense down-regulation of calpain-2 decreases prostate tumor invasiveness in mice*

Mice injected with PA or WT DU-145 cells expressing calpain-2 minigene (C2AS) were compared with mice receiving cells transfected with the vector alone (V). Results are the average of diaphragm score of 9 mice *versus* 8 for PA cells and 4 *versus* 3 for WT cells.

	V PA DU145	C2AS PA DU145	V WT DU145	C2AS WT DU145
Diaphragm tumors	9/10	8/10	4/5	3/5
Diaphragm invasiveness	2.33	1.13[a]	3.50	1.67[b]

[a] $P < 0.05$.
[b] $P < 0.10$.

Table 3 *Calpain expression does not differ in human prostate cancers based on tumor invasiveness*

Probe set	Description	Average of AC[a]	Average of OCC	Average of ND	AC/ND	*P*	AC/OCC	*P*
33384	Calpastatin	64.228	68.457	67.957	0.9451	0.6445	0.9382	0.8002
33385_g	Calpastatin	288.345	298.095	324.826	0.8877	0.1824	0.9673	0.4202
33908_	Calpain-1	2,485.08	2,451.91	2,356.19	1.0547	0.785	1.0135	0.9962
37001_	Calpain-2	1,560.52	1,507.79	1,751.10	0.8912	0.1428	1.035	0.7373
47510_r	CAST Calpastatin	293.507	288.238	256.426	1.1446	0.3642	1.0183	0.9132

[a] AC, aggressive prostate cancer ($n = 29$); OCC, organ-confined prostate cancer ($n = 24$); ND, normal prostate donor ($n = 23$).

translate to the human clinical situation. We surveyed 53 specimens from human prostate tumors and normal prostate tissue. Segregated by tumor stage, invasiveness, and metastases, we found no significant differences in mRNA levels of these tissues. This is in contradistinction to a recent report in which calpain-2 mRNA was found to be mildly (1.4 times) up-regulated in prostate carcinomas in conjunction with cadherin cleavage (50). We did not note this increased transcript level in our series of tumors, although the reasons for this discrepancy are not evident at present. However, in a different tissue, calpain-2 levels were not increased over that in normal skin in either squamous or basal cell carcinomas (51). Another calpain isoform reported altered in tumors, calpain-9 (31) is not reliably detectable in our prostate tissues: neither normal donor nor tumor (data not shown). According to accepted models of calpain activation (14, 15, 25), the lack of transcriptional change is not unexpected. Calpains appear to be activated at a post-translational level with calcium or other mechanisms, such as coactivators or phosphorylation (52–54),[4] being the operative event. In fact, in studies that attempt to exogenously express calpains, one usually fails to attain even a doubling of calpain levels, as higher activity leads to apoptosis (55). Thus, to demonstrate increased calpain activation in invasive tumors would require a way to assess *in situ* activation. For live cells, this can be accomplished by fluorescent substrates (Fig. 2). However, in nonliving cells we need to develop reagents to detect either the post-translational modifications that mark activation or colocalization of the activator cofactors.

In summary, we found that targeting calpain can limit prostate cancer cell invasiveness both *in vitro* and *in vivo*. This was likely because of the inhibition of rear deadhesion during growth factor-induced motility. In fact, CI-1 limits EGFR-mediated deadhesion of DU145 cells (data not shown) similar to the calpain-dependent detachment of fibroblasts (17) and epithelial keratinocytes (21). Our operative model of calpain function during tumor invasion posits an epigenetic or post-translational activation of calpain-2 rather than significant changes in protein levels. A survey of mRNA profiles of human prostate carcinoma specimens supports this by failing to demonstrate calpain gene expression differences between invasive and noninvasive carcinomas. However, to fully demonstrate the validity of this model will require a knowledge of how calpain-2 is activated and development of tools to detect such changes in activation. Additionally, the targeting of calpain-2 as a rational therapeutic intervention strategy will also necessitate new reagents, isoform-specific inhibitors. Because of the high degree of homology at the amino acid and structure levels (25) molecular agents offer the greatest hope of discriminatory agents. Thus, the full exposition of this potential novel target to limit tumor progression will rely as much on technical developments as on biological insights.

ACKNOWLEDGMENTS

Diana Whaley was invaluable in the successful completion of the *in vivo* studies. We thank Hidenori Shiraha, Angelu Glading, and John Gilbertson for important insights and suggestions.

REFERENCES

1. Jemal, A., Thomas, A., Murray, T., and Thun, M. Cancer Statistics, 2002. CA Cancer J. Clin., *52:* 23–47, 2002.
2. Morton, R. A. Management of clinically localized prostate cancer, U. S. Medicine, *36:* S4–7, 2000.
3. Chay, C., and Smith, D. C. Adjuvant and neoadjuvant therapy in prostate cancer. Semin. Oncol., *28:* 3–12, 2001.
4. Coffey, D. S. Prostate cancer metastasis: talking the walk, Nat. Med., *2:* 1305–1306, 1996.
5. Wells, A. Tumor invasion: role of growth factor-induced cell motility. Adv. Cancer Res., *78:* 31–101, 2000.
6. Levine, M. D., Liotta, L. A., and Stracke, M. L. Stimulation and regulation of tumor cell motility in invasion and metastasis. *In:* I. D. Goldberg and E. M. Rosen (eds.), Epithelial-Mesenchymal Interactions in Cancer. Basel, Switzerland: Birkhauser Verlag, 1995.
7. Wells, A., Kassis, J., Solava, J., Turner, T., and Lauffenburger, D. A. Growth factor-induced cell motility in tumor invasion. Acta Oncologica, *41:* 124–130, 2002.
8. Wyckoff, J. B., Jones, J. G., Condeelis, J. S., and Segall, J. E. A critical step in metastasis: *in vivo* analysis of intravasation at the primary tumor. Cancer Res., *60:* 2504–2511, 2000.
9. Condeelis, J. S., Wyckoff, J., and Segall, J. E. Imaging of cancer invasion and metastasis using green fluorescent protein. Eur. J. Cancer, *36:* 1671–1680, 2000.
10. Farina, K. L., Wyckoff, J. B., Rivera, J., Lee, H., Segall, J. E., Condeelis, J. S., and Jones, J. G. Cell motility of living cells visualized in living intact primary tumors using green fluorescent protein. Cancer Res., *58:* 2528–2532, 1998.
11. Lauffenburger, D. A., and Horwitz, A. F. Cell migration: a physically integrated molecular process. Cell, *84:* 359–369, 1996.
12. Wells, A., Gupta, K., Chang, P., Swindle, S., Glading, A., and Shiraha, H. Epidermal growth factor receptor-mediated motility in fibroblasts. Microsc. Res. Tech., *43:* 395–411, 1998.
13. Stupack, D. G., and Cheresh, D. A. Get a ligand, get a life: integrins, signalling and cell survival. J. Cell Sci., *115:* 3729–3738, 2002.
14. Glading, A., Lauffenburger, D. A., and Wells, A. Cutting to the chase: calpain proteases in cell migration. Trends Cell Biol., *12:* 46–54, 2002.
15. Perrin, B. J., and Huttenlocher, A. Calpain. Int. J. Biochem. Cell Biol., *34:* 722–725, 2002.
16. Huttenlocher, A., Palecek, S. P., Lu, Q., Zhang, W., Mellgren, R. L., Lauffenburger, D. A., Ginsburg, M. H., and Horwitz, A. F. Regulation of cell migration by the calcium-dependent protease calpain. J. Biol. Chem., *272:* 32719–32722, 1997.
17. Glading, A., Chang, P., Lauffenburger, D. A., and Wells, A. Epidermal growth factor receptor activation of calpain is required for fibroblast motility and occurs via an ERK/MAP kinase signaling pathway. J. Biol. Chem., *275:* 2390–2398, 2000.
18. Shiraha, H., Gupta, K., Glading, A., and Wells, A. IP-10 inhibits epidermal growth factor-induced motility by decreasing epidermal growth factor receptor-mediated calpain activity. J. Cell Biol., *146:* 243–253, 1999.
19. Palecek, S., Huttenlocher, A., Horwitz, A. F., and Lauffenburger, D. A. Physical and biochemical regulation of integrin release during rear detachment of migrating cells. J. Cell Sci., *111:* 929–940, 1998.
20. Sorimachi, H., Ishura, S., and Suzuki, K. Structure and physiological function of calpains. Biochem. J., *328:* 721–732, 1997.
21. Satish, L., Yates, D., Wells, A. Glu-Leu-Arg-negative CXC chemokine interferon γ inducible protein-9 as a mediator of epidermal-dermal communication during wound repair. J. Investig. Dermatol., *120:* 1110–1117, 2003.
22. Kassis, J., Radinsky, R., and Wells, A. Motility is rate-limiting for invasion of bladder carcinoma cell lines. Int. J. Biochem. Cell Biol., *34:* 262–275, 2002.
23. Kassis, J., Moellinger, J., Lo, H., Greenberg, N., Kim, H-G., and Wells, A. A role for phospholipase C-γ-mediated signaling in tumor cell invasion. Clin. Cancer Res., *5:* 2251–2260, 1999.
24. Turner, T., VanEpps-Fung, M., Kassis, J., and Wells, A. Molecular inhibition of PLCγ signaling abrogates DU-145 prostate tumor cell invasion. Clin. Cancer Res., *3:* 2275–2282, 1997.
25. Sorimachi, H., and Suzuki, K. The structure of calpain. J. Biochem., *129:* 653–664, 2001.
26. Hosfield, C. M., Elce, J. S., Davies, O. K., and Jia, Z. Crystal structure of calpain reveals the structural basis for Ca^{2+}-dependent protease activity and a novel model of enzyme activation. EMBO J., *18:* 6880–6889, 1999.
27. Strobl, S., Fernandez-Catalan, C., Braun, M., Huber, R., Masumoto, H., Nakagawa, K., Irie, A., Sorimachi, H., Bourenkow, G., Bartunik, H., Suzuki, K., and Bode, W. The crystal structure of calcium-free human m-calpain suggests an electrostatic switch mechanism for activation by calcium. Proc. Natl. Acad. Sci. USA, *97:* 588–592, 2000.
28. Moldoveanu, T., Hosfield, C. M., Lim, D., Elce, L. S., Jia, Z., and Davies, P. L. A Ca(2+) switch aligns the active site of calpain. Cell, *108:* 649–660, 2002.
29. Wang, K. K. Calpain and caspase: can you tell the difference? Trends Neurosci., *23:* 20–26, 2000.
30. Braun, C., Engel, M., Seifert, M., Theisinger, B., Seitz, G., Zang, K. D., and Welter, C. Expression of calpain I messenger RNA in human renal cell carcinoma: correlation with lymph node metastasis and histological type. Int. J. Cancer, *84:* 6–9, 1999.
31. Yoshikawa, Y., Mukai, H., Hino, F., Asada, K., and Kato, I. Isolation of two novel genes, down-regulated in gastric cancer. Jpn. J. Cancer Res., *91:* 459–463, 2000.
32. Liu, K., Li, L., and Cohen, S. N. Antisense RNA-mediated deficiency of the calpain protease, nCL-4, in NIH3T3 cells is associated with neoplastic transformation and tumorigenesis. J. Biol. Chem., *275:* 31093–31098, 2000.
33. Busquets, S., Garcia-Martinez, C., Alvarez, B., Carbo, N., Lopez-Soriano, F. J., and Argiles, J. M. Calpain-3 gene expression is decreased during experimental cancer cachexia. Biochim. Biophys. Acta, *1475:* 5–9, 2000.
34. Stone, K., Mickey, D. D., Wunderli, H., Mickey, G. H., and Paulson, D. F. Isolation of a human prostate carcinoma cell line (DU145). Int. J. Cancer, *21:* 274–281, 1978.
35. Xie, H., Turner, T., Wang, M-H., Singh, R. K., Siegal, G. P., and Wells, A. *In vitro* invasiveness of DU-145 human prostate carcinoma cells is modulated by EGF receptor-mediated signals. Clin. Exp. Metastasis, *13:* 407–419, 1995.
36. Turner, T., Chen, P., Goodly, L. J., and Wells, A. EGF receptor signaling enhances *in vivo* invasiveness of DU-145 human prostate carcinoma cells. Clin. Exp. Metastasis, *14:* 409–418, 1996.

[4] Unpublished observations.

37. Stracher, A. Calpain inhibitors as therapeutic agents in nerve and muscle degeneration. Ann. N. Y. Acad. Sci., *884:* 1999.
38. Badalamente, M. A., and Stracher, A. Delay of muscle degeneration and necrosis in mdx mice by calpain inhibition. Muscle Nerve, *23:* 106–111, 2000.
39. Ariyoshi, H., Okahara, K., Sakon, M., Kambayashi, J., Kawashima, S., Kawasaki, T., and Monden, M. Possible involvement of m-calpain in vascular smooth muscle cell proliferation. Arterioscler. Thromb. Vasc. Biol., *18:* 493–498, 1998.
40. Chen, P., Gupta, K., and Wells, A. Cell movement elicited by epidermal growth factor receptor requires kinase and autophosphorylation but is separable from mitogenesis. J. Cell Biol., *124:* 547–555, 1994.
41. Chen, J., and Iyengar, R. Suppression of ras-induced transformation of NIH 3T3 cells by activated $G\alpha_s$. Science (Wash. DC), *263:* 1278–1281, 1994.
42. Crawford, C., Mason, R. W., Wikstrom, P., and Shaw, E. The design of peptidyldiazomethane inhibitors to distinguish between the cysteine proteinases calpain II, cathepsin L and cathepsin B. Biochem. J., *253:* 751–758, 1988.
43. Umezawa, H. Structures and activities of protease inhibitors of microbial origin. Methods Enzymol., *45:* 678–695, 1976.
44. McCawley, L. J., O'Brien, P., and Hudson, L. G. Epidermal growth factor (EGF)- and scatter factor/hepatocyte growth factor (SF/HGF)-mediated keratinocyte migration is coincident with induction of matrix metalloproteinase (MMP)-9. J. Cell. Physiol., *176:* 255–265, 1998.
45. Glading, A., Uberall, F., Keyse, S. M., Lauffenburger, D. A., and Wells, A. Membrane proximal ERK signaling is required for M-calpain activation downstream of EGF receptor signaling. J. Biol. Chem., *276:* 23341–23348, 2001.
46. Kim, H., Turner, T., Kassis, J., Souto, J., and Wells, A. EGF receptor signaling in prostate development. Histol. Histopathol., *14:* 1175–1182, 1999.
47. Hirose, K., Kadowaki, S., Tanabe, M., Takeshima, T., and Iino, M. Spatiotemporal dynamics of inositol 1, 4, 5-trisphosphate that underlies complex Ca^{2+} mobilization patterns. Science (Wash. DC), *284:* 1527–1530, 1999.
48. Kulkarni, S., Goll, D. E., and Fox, J. E. Calpain cleaves RhoA generating a dominant-negative form that inhibits integrin-induced actin filament assembly and cell spreading. J. Biol. Chem., *277:* 24435–24441, 2002.
49. Babu, M., and Wells, A. Dermal-epidermal communication in wound healing. Wounds, *13:* 183–189, 2001.
50. Rios-Doria, J., Day, K. C., Kuefer, R., Rashid, M. G., Chinnaiyan, A. M., Rubin, M. A., and Day, M. L. The role of calpain in the proteolytic cleavage of E-cadherin in prostate and mammary epithelial cells. J. Biol. Chem., *278:* 1372–1379, 2003.
51. Reichrath, J., Walter, C., Mitschele, T., Classen, U., Meineke, V., Tilgen, W., and Seifert, M. Different expression patterns of calpain isozymes 1 and 2 (CAPN1 and 2) in squamous cell carcinomas (SCC) and basal cell carcinomas (BCC) of human skin. J. Pathol., *199:* 509–516, 2003.
52. Averna, M., deTullio, R., Passalacqua, M., Salamino, F., Pontremoli, S., and Melloni, E. Changes in intracellular calpastatin localization are mediated by reversible phosphorylation. Biochem. J., *354:* 25–30, 2001.
53. Melloni, E., Michetti, M., Salamino, F., Minafra, R., and Pontremoli, S. Modulation of the calpain autoproteolysis by calpastatin and phospholipids. Biochem. Biophys. Res. Commun., *229:* 193–197, 1996.
54. Melloni, E., Averna, M., Salamino, F., Sparatore, B., Minafra, R., and Pontremoli, S. Acyl-CoA-binding protein is a potent m-calpain activator. J. Biol. Chem., *275:* 82–86, 2000.
55. Shiraha, H., Glading, A., Chou, J., Jia, Z., and Wells, A. Activation of m-calpain (calpain II) by epidermal growth factor is limited by PKA phosphorylation of m-calpain. Mol. Cell. Biol., *22:* 2716–2727, 2002.

PROTEIN KINASE C SIGNALING IN THE HUMAN PROSTATE CANCER CELL LINE DU-145 AFTER EXPOSURE TO AN LHRH ANALOG.

Karlyn J. Bailey, Ahmed Hassan, Alan Wells* and Timothy Turner. Tuskegee University, Tuskegee, Alabama and *University of Pittsburgh, Pittsburgh, Pennsylvania.

Analogs to luteinizing hormone releasing hormone (LHRH) have been shown to have antiproliferative actions on the human, androgen-independent prostate cell line, DU-145. Although the mechanism by which these analogs exert their antiproliferative effect is unknown, DU-145 cell growth and invasion are known to be mediated through the epidermal growth factor receptor (EGFR). We have hypothesized that the antiproliferative effects of LHRH analogs are mediated through negative attenuation of the EGFR via protein kinase C (PKC) activation. PKC activation in turn limits EGFR tyrosine kinase activity by phosphorylating the EGFR at amino acid threonine 654. The objective of this study was to determine whether Cetrorelix, an LHRH antagonist, attenuates EGFR signaling via PKC-mediated transmodulation. In this study, one subline over-expresses a full length EGFR (Wild Type-WT) the other subline over-expresses a full length EGFR in which amino acid threonine 654 was mutated to an alanine making it resistant to PKC phosphorylation (Wild Type A^{654} -WT A^{654}). Dose response studies conducted on the WT DU-145 subline with PKC activator PMA resulted in significant growth reduction at 10^{-5} M. No significant growth inhibition was witnessed in the WT A^{654} subline exposed to PMA. The PKC inhibitor chelerythrine chloride (10^{-6} M), in the presence of PMA (10^{-5} M) alleviated the inhibition caused by PMA. Treatment of WT A^{654} with Cetrorelix, resulted in a significant inhibition of growth in this subline at 10^{-4} M. Co-treatment of both DU-145 sublines with chelerythrine chloride failed to alleviate this inhibition of growth.

Key words: DU-145 cells, Cetrorelix, PKC, EGFR, Prostate Cancer

Karlyn J. Bailey, Ahmed Hassan, Alan Wells and Timothy Turner (2002). *Protein Kinase C Signaling In The Human Prostate Cancer Cell Line DU-145 After Exposure To An LHRH Analog.* Abstract-Research Centers in Minority Institutions (RCMI) 2002 Spring Symposium, Jackson, MS

An organotypic model for prostate tumor metastasis.

Clayton Yates, Donna Stolz, Linda Griffith*, Alan Wells, University of Pittsburgh and MIT*

Prostate cancer metastasis is among the leading deaths of American males in the United States. Development of cancer *in situ* has plausible and treatable means. However, the molecular mechanisms contributing to the initiation, progression and ultimate development of androgen independent carcinomas that have the ability to metastases to distal sites such as lung, diaphragm, bone marrow, brain and liver are currently poorly understood (Holleran, 2002). This lack of understanding is due in part to the lack of *ex vivo* metastasis and invasion experimental systems that fully recapitulate the pathophysiological events of this disease. Recently, we have developed a three dimensional liver perfusion culture, which allows for *in situ* observation and ensures a relatively homogeneous distribution of flow and mass transfer throughout the system to meet the metabolic demands of the livers cells augmented by an appropriate scaffold which facilitates morphogenesis of primary cells into tissue-like structures (Powers et al, 2002). This system, formally named a Micro-fabricated Array Bioreactor, affords for the recreation of an *in vivo* environment for *in vitro* observation and provides for an optimal device for the study of physiological events. In order to examine cancer metastasis and invasion we utilized this system. Hepatocytes were obtained from established liver perfusion protocols (Powers et, 2002, Block et al. 1996; Wu et al., 1996). Day 3, 200um spheroids were introduced into the reactor. After allowing 5 days of observed hepatic tissue morphogenesis from spheroids, an endogenously GFP expressing DU-145 WT human prostate cancer cell line genetically engineered to over-express a full length EGFR, which is very invasive, was introduced into the reactor by identical methods as spheroids. *In situ* observation of the co-culture system was observed by light microspopy over a 30 day period and subsequent two-photon scanning fluorescence microcopy and transmission electron microscopy. *In situ* observation of co-cultures revealed cell proliferation of DU-145 WT was observed after only 4 days, with an overgrowth of DU-WT cells from 14 days. The bioreactor medium did not support growth of DU-WT cells in the absence of hepatocytes. The overflowing DU-145 WT migrated across the silica and invaded adjacent hepatocyte filled channels. TEM experiments show that DU-145 WT cells invade the hepatocyte parenchyma within the 30 day incubation. Although only preliminary, these experiments provide the basis for the development of an *ex vivo* model system in which to observe and potentially dissect the dynamic process of tumor invasion and metastasis.